Design for Additive Manufacturing

Zander Bratland

William Austrheim

Bachelor’s thesis in Mechanical engineering

Bergen, Norway 2023

Høgskulen på Vestlandet

Design for Additive Manufacturing

Zander Oksavik Bratland

William Austrheim

Department of Mechanical- and Marine Engineering

Western Norway University of Applied Sciences

NO-5063 Bergen, Norway

IMM [2023]-M[11]

Høgskulen på Vestlandet

Fakultet for Ingeniør- og Naturvitskap

Institutt for maskin- og marinfag

Inndalsveien 28

NO-5063 Bergen, Norge

Norsk tittel:	Design for additiv tilvirkning
Author(s), student number:	William Austrheim, 591433
	Zander Oksavik Bratland, 591435
Study program:	Mechanical engineering
Date:	[06 2023]
Report number:	IMM 2023-M11
Supervisor at HVL:	Saeed Bikass, Associate Professor
Assigned by:	Bergen Engines, HVL
Contact person:	Saeeds Bikass
Antall filer levert digitalt:	*None*

Preface

This bachelor thesis was carried out within the Department of Mechanical and Marine Engineering at Western Norway University of Applied Sciences (WNUAS). The project was conducted as part of the Mechanical Engineering program.

We are grateful to our supervisor, Associate Professor Saeed Bikass, whose guidance proved invaluable throughout the entire thesis process. His support and constructive feedback greatly contributed to the successful completion of this thesis. We will extend our appreciation of the collaboration with Bergen Engines. Bergen Engines provided the case studies and valuable insights during the work on this thesis. We extend our appreciation to Sjur Herheim and Svein Eidsvik from Bergen Engines.

Abstract

This report will give an introduction and a deeper understanding of both the technology and the process of additive manufacturing itself, a method where different considerations are required compared to traditional manufacturing such as machining and casting. This project has been accomplished in cooperation with Bergen Engines, who provided critical engine parts which they wanted to have redesigned with a mindset of additive manufacturing. Some of the parts required retaining high stiffness or increased fatigue resistance, and weight reduction were commonly desired for all parts. The report explores both existing and new growing additive manufacturing technologies and methods, which will cover the unique design process that differ from the conventional methods. It includes up to date information of 3D printers using powder bed fusion, direct energy deposition, binder jetting, electron beam melting, and hybrid- and multimaterial printing. This thesis will focus on Powder bed fusion, as this is not only the most common additive manufacturing process, but also regarded as the best method for the case studies in this thesis.

Every part was redesigned using PTC's CAD software Creo Parametric which has a built-in generative design for topology optimization and lattice functions. The new generated geometries were all attempted analyzed in ANSYS finite element software for simulation of their real-life use and anticipated results. Most of the results had to be relied on Creo's optimization analysis as the geometries caused unknown errors making them unable to mesh or import into ANSYS at all.

Sammendrag

Denne oppgave skal gi en introduksjon og en dypere forståelse av både teknologien og selve prosessen ved additiv tilvirkning, en produksjonsmetode hvor det kreves helt andre hensyn sammenlignet med tradisjonelle tilvirkningsmetoder som maskinering og støping. Dette prosjektet er utført i samarbeid med Bergen Engines, som sørget for kritiske motordeler de ønsket å få tilpasset og forbedret med en tankegang ut fra additiv tilvirkning. Noen av delene trengte å beholde høy stivhet eller økt tretthetsmotstand, og vektreduksjon var ønsket for alle delene. Oppgaven utforsker både eksisterende og nye voksende teknologier og metoder innenfor additiv tilvirkning, og handler om den unike designprosessen som skiller seg fra de konvensjonelle metodene og hvordan designet kan tilpasses for å dra nytte av fordelene med 3D-printing. Den inkluderer oppdatert informasjon om 3D-printere som bruker teknologi som powder bed fusion, direct energy deposition, binder jetting, electron beam melting, og hybrid- og mulitmaterial printing.

Hver del ble redesignet ved hjelp av PTCs CAD-programvare Creo Parametric, som har en innebygd generativ design for topologioptimalisering og latticefunksjoner. De nye genererte geometriene ble alle forsøkt analysert i ANSYS elementmetode-programvare for simulering av deres virkelige bruk og forventede resultater. De fleste av resultatene måtte baseres på Creo sin optimaliseringsanalyse, da geometriene gjentatte ganger forårsaket ukjente feil i ANSYS som gjorde at de ikke var i stand til å meshe eller importere til ANSYS i det hele tatt.

Table of contents

Preface V

Abstract VII

Sammendrag IX

Nomenclature XIII

1. Introduction 1

1.1 Motivation 1

1.2 Objectives 1

1.3 Bergen Engines 2

2. Literature review 3

2.1 Powder bed fusion 3

2.2 Materials for metal AM 4

2.2.1 Benefits and drawbacks of AM 5

2.3 Design for additive manufacturing 5

2.3.1 Recommendations for DFAM 5

2.3.2 Topology optimization 6

2.3.3 Lattices 7

2.4 Multi-material Additive manufacturing 7

2.5 Hybrid AM 8

2.5.1 Hybrid AM by machining and peening 8

2.5.2 Ultrasonic additive manufacturing 9

3. Method 10

3.1 Topology optimization 10

3.2 Finite element method 12

3.3 Lattice 13

4. Case studies 14

4.1 Case 1 Lifting tool for turbocharger foot 14

4.2 Case 2 Nozzle holder housing 15

4.3 Case 3: Injection cam follower 16
4.4 Case 4: Valve bridge 18
5. Case study results 20
5.1 Case 1 Lifting tool for turbocharger foot 20
5.1.1 Design 20
5.1.2 Results 22
5.2 Case 2 Nozzle Holder Housing 33
5.2.1 Redesign 33
5.2.2 Results 35
5.3 Case 3 Injection cam follower redesign 37
5.3.1 Redesign 37
5.3.2 Shell model 37
5.3.3 Topology optimization 37
5.3.4 Modification of original geometry 39
5.3.5 Results 41
5.4 Case 4 Valve Bridge 45
5.4.1 Redesign 45
5.4.2 Results 48
6. Discussion 52
6.1 Case 1, Lifting tool 52
6.2 Case 2, Nozzle holder housing 53
6.3 Case 3, Injection cam follower 53
6.4 Case 4, Valve bridge 54
7. Conclusion 55
8. References 56
List of figures 58
List of tables 61

Nomenclature

AM	Additive Manufacturing
TO	Topology Optimization
BE	Bergen Engines
PBF	Powder Bed Fusion
CM	Conventional Manufacturing
EBM	Electron Beam Melting
MLS	Metal Laser Sintering
TPMS (lattice)	Triply periodic minimal surface (lattice)
LPS	Liquid Phase Sintering
DFAM	Design For Additive Manufacturing
UAM	Ultrasonic Additive Manufacturing
MMAM	Multi-Material Additive Manufacturing
DED	Direct Energy Deposition
FEA	Finite Element Analysis

1. Introduction

Additive manufacturing (AM), also known as 3D printing, is a rapidly growing field that allows for the creation of complex parts and structures by building them up layer by layer. Unlike traditional manufacturing methods, which involve removing material from a larger piece to create the final product, additive manufacturing adds material to create the final product. This allows for greater design freedom, less wasted material, faster prototyping, and the ability to create complex geometries that would be difficult or impossible to produce using traditional methods. Additionally, the use of digital designs and computer-controlled fabrication allows for greater precision and repeatability in the production process. The technology can be used in a wide range of industries, including aerospace, healthcare, and automotive, and has the potential to revolutionize the way products are designed and manufactured. It is an important topic to research, in various engineering and product design fields.

Despite the many benefits of additive manufacturing, there are also significant challenges that must be addressed. One major challenge is the limited range of materials that can be used in the process, which is limiting the type of products that can be produced. Additionally, the precision and repeatability of the process can be affected by factors such as temperature and humidity, and the finished products can also be subject to issues like warping and shrinkage. The technology also requires high capital costs, also it can be challenging to scale up the technology for mass production and end-use parts. These are important topics to consider when researching additive manufacturing.

1.1 Motivation

The ability to create complex parts and structures by building them up layer by layer, rather than by removing material from a larger piece, has already led to significant advances in a wide range of industries, including aerospace, healthcare, and automotive. Additionally, the use of digital designs and computer-controlled fabrication allows for greater precision and repeatability in the production process. As such, there is a growing need for research in this area to fully understand and exploit the capabilities of additive manufacturing.

The main challenges will be to combine distinctive designs and materials for optimizing structure, weight, and efficiency. Thus, it requires a new and unique way of thinking and planning design to fully exploit the capabilities of AM and topology optimization (TO). As an example, an optimization process might involve combining and simplifying the design to also include multiple materials for increased efficiency if found so. The result of over-engineering is not an uncommon occurrence. Implementing an AM approach can therefore lead to more sustainable solutions.

A bachelor thesis on this topic could explore the various applications of additive manufacturing in different industries. It could investigate ways to improve the technology and material options to achieve desired properties and mechanical features, or even study the impacts on the environment and economy. This research will be valuable for understanding the potential of additive manufacturing and identifying areas where further development is needed to fully realize its benefits.

1.2 Objectives

The objectives of this project will be to investigate the potential of additive manufacturing and gain knowledge about the AM process, design and materials. Additionally, the project aims to explore the use of optimization methods to reduce weight, material usage, and improve product sustainability. The acquired knowledge will be applied to case studies provided by Bergen Engines (BE). The case studies given consists of four cases with their unique functions and challenges. Design for additive manufacturing will be utilized to solve these challenges and create an improved design.

1.3 Bergen Engines

Bergen Engines is a Norwegian company that designs, develops, and manufactures medium-speed gas and diesel engines for power generation, marine propulsion, and offshore drilling applications. The company was founded in 1855 and has since 1946 built engines to later become a global leader in the engine industry. Bergen Engines' product portfolio includes a range of four-stroke engines with power outputs ranging from 1.4 MW to 12 MW. The engines are designed to run on a variety of fuels, including natural gas, biogas, diesel and heavy fuel oil.

The company has a strong focus on sustainability and offers engines that comply with the latest environmental regulations, such as IMO Tier III and EU Stage V. Bergen Engines' engines are known for their high efficiency, reliability, and low emissions. In 1999, Rolls-Royce PLC acquired Bergen Engines and later in 2013 integrated into Rolls-Royce Power Systems. Bergen Engines was then acquired by Langley Holdings PLC from Rolls-Royce PLC in 2021, which even further strengthened the company's position in the engine market [1].

They have provided four cases to focus on, a cam follower injection pump, a valve bridge, a nozzle holder housing, and a lifting tool for a turbocharger foot. The first three parts are all critical components within the same engine machinery.

2. Literature review

Additive manufacturing is constantly growing and improving. This thesis will explore both existing and emerging technology relevant to the case study. Materials and design choices for AM will also be considered.

2.1 Powder bed fusion

Powder bed fusion (PBF) stands out as one of the leading additive manufacturing technologies for metals. PBF is the preferred AM technology when parts with high detail, good surface finish, and low anisotropy are required. The ability to also print polymers, ceramics, and composites makes it a very versatile technology [2, p. 125].

When manufacturing metals with PBF, the two process variants that are often used is metal laser sintering (mLS) and electron beam melting (EBM). The mLS process takes place inside a closed chamber filled with inert gas, usually nitrogen. This reduces the degradation of the metal powder and oxidation. A thin layer of powder is spread evenly across the build surface with a counter-rotating roller. The powder is then fused by a co2 laser beam. Galvanometers move the laser to form a cross-section of the part being produced. The build platform is lowered by one layer and the process is repeated. The temperature during the mLs process is critical. Metal powder in the build platform is heated, reducing the required energy for the laser to melt the powder. Proper heating and cooling reduce warping and internal stresses in the part [2, pp. 126–127]. Figure 1 shows the PBF process.

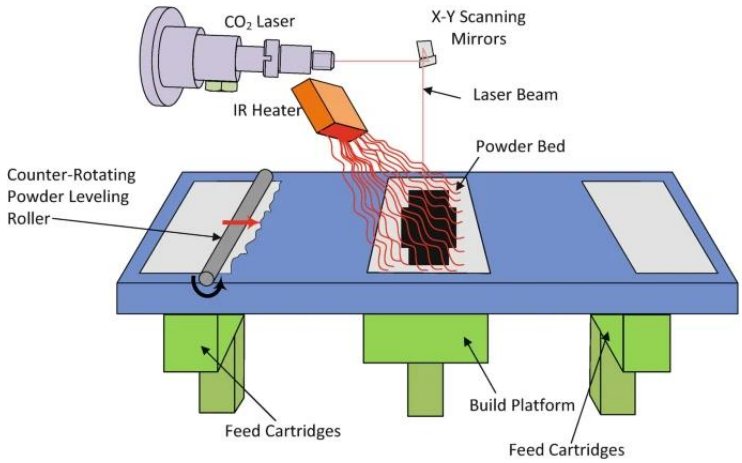

Figure 1 Illustration of PBF process [2, p.126]

EBM is similar to mLS, but with some important differences. Electron beams heat the powder with kinetic energy, while the laser heats it through photon absorption. This requires a conductive metal to avoid powder particles being too negatively charged. Two of the big advantages for EBM are the high print speed and lower residual stress in printed parts due to the elevated bed temperature. This reduces the need for support structures and leads to more efficient production [2, pp. 159–162].

With PBF there are two powder fusion mechanisms typically used for metals, full melting and liquid phase sintering. Full melting means that the powder on the print bed is fully melted, exceeding the layer thickness and melts a portion of the previous layer. Creating a well-bonded and high-density structure. Full melting is often used with engineering alloys due to the favorable mechanical properties caused by the rapid melting and cooling of the metal [2, p. 138].

Liquid phase sintering (LPS) is a more flexible mechanism than full melting. In this process, the metal powder is heated such that only a portion of the powder is melted. The melted powder glues the

remaining solid particles together. One major benefit of LPS is that particles with a high melting point can be fused without melting or sinter them directly [2, p. 134].

2.2 Materials for metal AM

To produce high-quality metal AM parts, good materials are important. Metals processed by AM technologies are available in different forms, such as powder, wire and strip metal. This chapter will provide an overview of some of the most common materials for metal AM and their mechanical properties.

It is important to note that when comparing a metal (titanium, steel, aluminum alloy) AM part to a conventionally manufactured (CM) counterpart, the mechanical properties may not be the same. Due to the finer microstructure in the AM part, the tensile properties can in many cases be significantly higher than their CM counterpart [3, pp. 384–386]. However, the AM process can introduce unwanted properties like porosity and defects to the part. Studies have shown that properties such as ductility, fatigue and endurance limit tend to be lower for AM parts than their CM counterparts [4, p. 23].

The titanium alloy Ti-6Al-4V is the most common and widely used within AM. It is composed of 6% aluminum and 4% vanadium, with the remainder being titanium. It is also known as Grade 5 titanium accounting for about 50% of all titanium used in various industries. This alloy is valued for its high strength-to-weight ratio, excellent corrosion resistance, and biocompatibility, making it ideal for use in the aerospace, automotive, medical and sports industries. It is also frequently used in the manufacturing of surgical implants, such as hip and knee replacements.

It goes to say that titanium and its alloys in general are very hard to machine, this is due to its low ductility, high tensile and yield strength, lower modus of elasticity and thermal conductivity than its heavier counterpart steel [5, p. 4642]. Because of this, titanium is sought to be a leading material to be used in AM rather than conventional subtractive manufacturing. Powder metallurgy (PM) is a cost-effective method of producing titanium components. This contributes to titanium being the most common metal used in AM.

Aluminum, while being a more inexpensive metal, is less cost-effective compared to its performance from AM. Machining aluminum is a much easier task hence being softer, therefore demanding less energy to manufacture that way.

Nickel-based superalloys are high-performance materials that are widely used in the aerospace, power generation, and petrochemical industries due to their excellent combination of high strength, corrosion resistance, and high-temperature performance. The unique properties of nickel-based superalloys make them ideal for use in extreme environments, such as those found in gas turbines, jet engines, and rocket propulsion systems. With densities between 8-8,9 g/cm3, it is generally heavier than steel but often provides higher tensile and yield strength and is usually harder. At temperatures above 540 °C, these superalloys are typically utilized since at these temperatures, regular steel and titanium alloys start to lose their strength and steels start to corrode more frequently. Superalloys maintain their mechanical strength, thermal creep resistance, surface stability, and corrosion or oxidation resistance at high temperatures. Depending on the alloy's composition, some alloys can survive temperatures higher than 1200°C. Although grain boundaries could increase strength, they also reduce creep resistance, which is why superalloys are frequently formed as a single crystal [6].

Steel is a frequently material used within AM and there are many options available. 316L stainless steel is a commonly used metal in AM due to its good mechanical properties and corrosion resistance. Great functionality in different temperatures makes it suitable for many applications as well [7, p.25]. 17-4PH stainless steel is another common steel for AM. It is a precipitation-hardening steel [8, p.281], which enables it to be hardened and have its mechanical properties enhanced by heat treatment. Table *1* contains material properties for the materials used in the case studies.

Table *1*: Material properties

	GJS-500-7 [9]	Al6061-T6 [10]	316L [7]	Ti-6Al-4V [5]	17-4PH [4]	AlSi10Mg [11]
Density (g/cm^3)	7,1	2,7	8	4,4	7,8	2,7
Ultimate tensile strength (MPa)	500	310	594	1095	1110	367
Yield strength (MPa)	320	276	485	990	1087	251
Youngs modulus (GPa)	169	68,9	165	112	199,5	73
Fatigue limit (MPa)	224	96,5	340	500	300	100

2.2.1 Benefits and drawbacks of AM

From the economic perspective, AM is unsuitable for larger batch production systems due to economies of scale, which are the inverse relationship between production and fixed cost per unit. However, for low-volume production, AM could be a viable alternative to traditional manufacturing (less than 40 pieces). AM provides a one-to-one economy, which means that it is possible to produce a single customized or complicated design at a low cost. Machines and materials for AM are currently expensive, but these costs will fall as AM becomes a more common manufacturing technology. AM is expected to become more cost-effective as larger production quantities become economically feasible.

An important part of the field includes the cost and material efficiency both considering additive manufacturing and traditional CNC manufacturing. There is a fine line in certain situations where the cost and efficiency tips in favor to either one. If a certain component requires extra strength where the possible material reduction optimization is minimal, it would not necessarily be any more efficient or less costly to use AM in favor to use CNC and machining off material.

One of the biggest advantages of AM in the lines of efficiency and weight saving, is the possible manufacturing of topology optimized parts, which is nearly impossible using traditional machining. This method creates parts that not only significantly save weight, but also save waste materials and generally use much less materials. It is estimated that metal powder not utilized during manufacturing has a recyclability of 95-98%.

The ability to manufacture directly from 3D CAD models also results in no transition expenses following the no longer needed requirement for tools and molds. These files may be shared, edited and customized easily without any more physical changes needed [12, pp.5-7].

2.3 Design for additive manufacturing

Some of the important aspects of Design for Additive Manufacturing (DfAM) will be covered in this chapter. DfAM involves taking advantage of the benefits the AM technology can offer, to produce a product. This can be done by redesigning an existing product, which is the main focus of this thesis, or to design a product from the ground up specifically for AM [13, p.41].

2.3.1 Recommendations for DFAM

AM can be expensive and time consuming compared to conventional manufacturing methods. It is therefore important that the AM parts add enough value, to make it worth the extra cost compared to a CM part [13, p.44]. For example, by utilizing the complex geometry enabled by AM to add extra features to the part, or to simplify a part. AM enables assemblies to be combined into a smaller number of parts, while maintaining or even improving the function of the product, often called part consolidation. Notable advantages of part consolidation are reduced time spent on assembly, less need for fasteners and tooling for assembly [2, p.567].

The orientation of the AM part during printing is very important to consider, as it can have a big effect on several other parameters. The part should usually be oriented to minimize the amount of overhang. A laser PBF printer can handle overhangs of 45 to 60 degrees, depending on the material used [13, p.158]. If this angle is exceeded, support structures must be used to avoid collapsing material. Supports are very useful, however they lead to more material use, print time and postprocessing [13, p.95]. The mechanical properties of AM parts suffer from some degree of anisotropy, depending on the AM technology used. There is a weakness between the print layers, degrading the strength in the vertical or z-direction [13, p.46]. If strength is important, this should be considered when choosing the optimal print orientation.

2.3.2 Topology optimization

The unique capabilities of DfAM allow the production of complex geometries, which is very hard or impossible with traditional methods. Several optimization methods take advantage of this, such as TO.

Conventional numerical design processes involve applying loads to a part that has already been manufactured and evaluating where it weakens. Engineers must then alter the design until the part meets the given mechanical constraints. With TO, the logic is different: the mechanical loads represent input data that will allow the software to propose a new geometry for the part. Therefore, there should be less iterations made to the design of the part, considerably reducing design and manufacturing lead times [14].

Topology optimization creates a design through an iterative process. For a given set of boundary conditions, the optimal design is discovered. This design satisfies the given performance requirements for example mass or stiffness, by distributing material where it is needed. Traditional manufacturing is not able to fully utilize topology optimization, due to the complex geometry and designs. Additive manufacturing is therefore well suited for this technology as it can produce complex parts in one single operation [2, p.514].

Recently, deep learning methods have been applied to topology optimization to enhance its efficiency and accuracy. These methods employ neural networks to learn the relationship between the design space and the material distribution, allowing for the generation of designs with high structural performance and complex topologies. However, these methods require a large amount of training data and can be sensitive to the choice of network architecture and hyperparameters [15, pp.1–5].

There are different methods available for topology optimization, which can be broadly classified into two main categories: density-based and level-set based methods. Density-based methods employ a density field to represent the material distribution within the design space. By using optimization algorithms to manipulate the density field, these methods generate designs with the desired structural performance while satisfying specific constraints. The solid isotropic material with penalization (SIMP) method is a popular choice in this category. It employs a penalty factor to penalize low-density materials and promote high-density ones, leading to designs with smooth material transitions. However, it may produce a large number of small features and can be sensitive to mesh density. The evolutionary structural optimization (ESO) method is another density-based method that employs a genetic algorithm to generate optimal designs. While this method can handle multiple load cases and generate designs with high structural performance, it can be computationally expensive.

On the other hand, level-set based methods use a level-set function to represent the geometry of a design. The material distribution is then obtained as a step function of the level-set function. These methods can handle complex topologies and generate designs with sharp features. The solid freeform fabrication with level sets (SFFLS) method is a popular choice in this category. It utilizes level sets to define the geometry and optimize the material distribution, leading to designs with both smooth and sharp features. However, this method can be computationally expensive and requires a large amount of memory[15] .

2.3.3 Lattices

Lattice structures are the most known type of infill in hollow parts or parts that needs more structural integrity without adding too much mass and therefore weight. Lattices can vary in complexity, from simple plain rods or beams to wavy shapes and nature-looking designs. It can be seen as repeating pattern structure filling up a volume or along a surface. In a similar matter to TO, lattices are also inspired by nature's fundamental building blocks, like biological lattices such as the internal structure of bones and honeycombs. The simplest repeating structure in a lattice is the unit cell. The type of lattice is determined by the unit cell structure. A cell map is used to arrange unit cells in space to form a lattice. Cell maps can be square, round, spherical, or curved to fit between two faces or any combination of these.

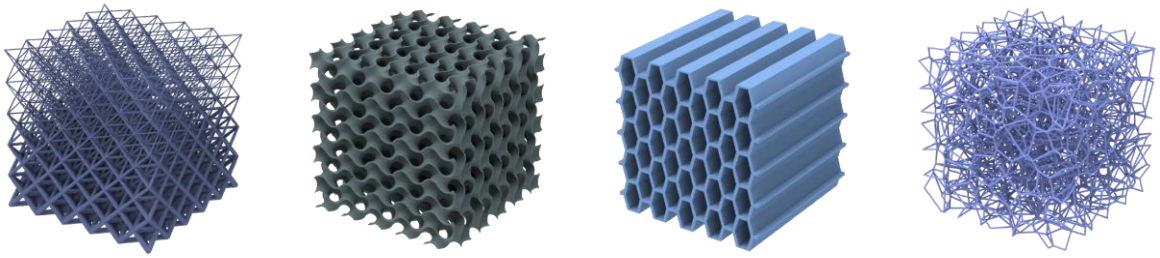

Figure 2 Four types of lattice structures [16]

The lattice to the left in Figure 2 shows an example of beam lattices at 45 degrees, but these beam lattices can have several different designs in any direction, depending on the desired properties. Beam lattices can generally offer a great stiffness-to-weight ratio or be elastic and compliant. The second lattice is a classic case of TPMS lattice, also known as gyroid. It is designed to retain great strength in all directions, offering all-round great mechanical properties. As opposed to the latter, the third lattice shows a honeycomb lattice, which is designed to offer high stiffness in one specific direction, making it relatively weak in other directions. Lastly, the fourth lattice represents stochastic lattice structures, where the positions, interactions, or properties of the elements or entities on the lattice are determined by random or probabilistic processes.

2.4 Multi-material Additive manufacturing

The process of multi-material additive manufacturing processes (MMAM) varies just as much as other AM methods, but there are three methods most commonly used for MMAM, material extrusion, PBF and material-jetting. One of the most popular AM methods is extrusion-based, which involves dispensing material feedstock through a single or many nozzles to allow the creation of multi-material 3D structures. Thermoplastics, metal-filled thermoplastics, composites, flexible elastomers, and blended multi-material powder-based feedstock are among the materials that this process is capable of printing.

The ME process components require post-AM de-binding and sintering to provide structural integrity. Moreover, the powder recycling and reuse procedure is rendered unnecessary because the binder is combined with the material rather than being extruded into a powder bed, saving both time and money. The printing resolution, which is based on the powder size and nozzle diameter, is the technology's primary drawback. As with Norsk Titanium which 3D prints titanium by extrusion system, or their patented Rapid Plasma Deposition, the resolution and printing shapes are quite rough, therefore post-machining is needed. Furthermore, manufacturing items with overhanging shapes and huge aspect ratios is difficult and necessitates a steady supply of feedstock as well as quick solidification. A multi-material feed-stock design is essential for achieving this.

When it comes to PBF, using blended materials has made it possible to achieve multi-material PBF. The main concern regarding this method is to ensure sufficient re-melting and achieving a lasting bond between the different materials. Strengthening the bond between layers opposes a challenge affected by

the different material powder properties and characteristics. The components are prone to exhibiting a lack of fusion due to the low-energy density of the heat source, whereby the high-melting-point alloying elements are located, or the applied energy density of the porosity remains unchanged due to the existing low-melting-point elements during the optimization of the process parameters to avoid undesirable defects. Otherwise, variations in the thermal characteristics are what induce cracks between different materials. For materials with high melting points, a method of using finer powder sizes has been developed to increase their surface area and degree of energy absorption during the PBF process [17, p.21].

Recycling powder in DED systems is more difficult compared to PBF. It is nearly impossible to recycle powders when using multiple materials in a machine. To separate different particles, a mixture can be placed in a centrifuge because of the difference in density of each material. The lighter powder particles will be concentrated near the center of the container, and particles with higher density will migrate toward the edge of the centrifuge barrel. However, small contamination can have devastating consequences, so recycling of this type can be challenging [2, p.399].

An example of an existing multi-material printing system is the small-scale mLS machine produced by the German company 3D-Micromac. They have created a small-scale mLS processes that use 40 mm-tall, 25–50 mm-diameter build cylinders. They have created a special two-material powder feeding system to use the tiny powder particle sizes required for fine feature replication. The build platform is situated between two cylinders for feeding powder. The powder is forced upward into the feeder, charging the hopper, when the spinning rocker arm is over a cylinder for feeding powder. Before laser processing, the powder is deposited and smoothed when the rocker arm is moved across the top of the build platform and away from the build cylinder. To create multi-material structures, it is possible to change the material being processed layer by layer by switching between feed cylinders [2,p.158].

2.5 Hybrid AM

Hybrid Manufacturing is an emerging technology, that combines AM with a secondary process such as conventional machining. This technology aims to achieve a greater result than the two processes can achieve on their own. Resulting in a product with less production cost, improved mechanical performance, better surface finish and tolerances [18, p.623].

2.5.1 Hybrid AM by machining and peening

Hybrid AM is commonly associated with machining or removal of material. The side walls of an AM part are usually machined to improve its surface finish and accuracy, and a layer's top surface can also be machined to prepare it for the next layer. Material is removed from every layer or in intervals, this allows the tool to easily machine all side walls [2, p. 353]. Hybrid AM by machining is best suited for the DED technology, as it is simpler to incorporate with machining tools compared to PBF [2, p.354].

Another secondary process is peening. During the printing process, the top surface of a layer is peened to improve the surface quality, microstructure and mechanical properties. Several different methods are available. Shot peening consists of high-velocity beads that deform, and work-harden the surface. This is best suited for DED. It is effective for PBF as well, however avoiding contamination in the powder bed is important [2,p.357].

Ultrasonic peening is a different peening technology that uses ultrasonic energy instead of kinetic energy from beads. It works by vibrating a tool against the surface of the part. This method shows good improvements in surface quality, microstructure, fatigue resistance and corrosion resistance. In addition, internal stresses are relieved [2,p.359].

2.5.2 Ultrasonic additive manufacturing

In hybrid manufacturing, a technique known as Ultrasonic Additive Manufacturing (UAM) combines ultrasonic welding and CNC machining. Complex, multi-material 3D components with embedded components are produced using this method. Metal strips are joined together using high-frequency sound waves to form a solid bond between the layers. Heat is also produced throughout the process, which aids in softening the metal and strengthening the bond. UAM enables parts to be CNC machined while they are printed, creating a very effective process. Compared to other additive manufacturing technologies, this one is affordable and has existed since 1999. Moreover, it is a low-temperature bonding method that makes it possible to combine several metals to create complicated components . The true finished shape is then machined with CNC machining, and it is possible to retain this entire process within the same machine. This method is also perfectly suitable for repairing components by both machining away damages and rebuilding the concerning areas with the printing head[19]. Figure 4 and Figure 3 show the process.

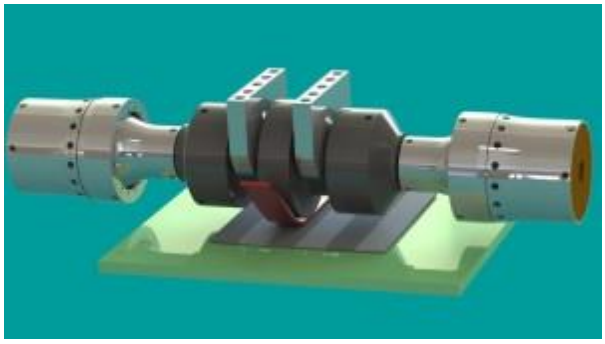

Figure 4 Bonding a metal strip to the base plate with UAM [20]

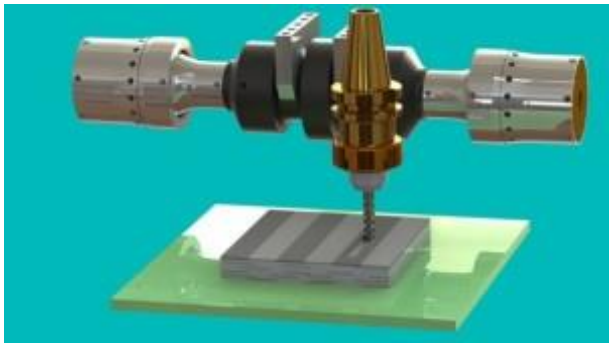

Figure 3 Periodic machining operations [20]

3. Method

3.1 Topology optimization

The software used for topology optimization is the Generative Design tool in Creo Parametric. STEP files for the four cases were provided by BE and imported to Creo. Several preparations must be made to the original geometry before the topology optimization analysis can start. First, the parts of the original design that must be kept intact is identified. This geometry is called preserved bodies and are created by copying the original geometry. Alternatively, if the goal is to create a new part from scratch, the required preserved bodies must then be created in this step. Only the geometry that is important to the functionality of the part should be kept as preserved body, such as the areas where loads and constraints are applied. Process shown in Figure 5.

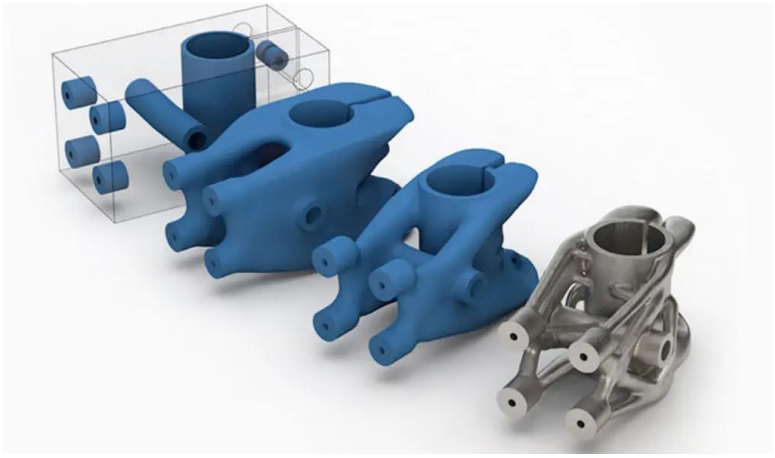

Figure 5 Topology optimization process [21]

To define the boundaries and initial shape of the design space that will be optimized, a starting geometry is created. Depending on the available space surrounding the part, the starting geometry should be spacious and extend well beyond the boundaries of the original part. If the starting geometry is too small, it can constrain where the geometry can be generated, limiting the optimization results. Excluded bodies is geometry that prevent any geometry to be generated in its place. Unlike preserved bodies, excluded bodies are not included in the generated design.

When the geometry is fully prepared, the constraints and loads can be defined. The available constraints in Creo are fixed support, displacement, cylindrical support and planar. The option “Add load case” is a useful feature that enables optimization with multiple loads and constraints at the same time.

The next important step in the optimization process is defining constraints and loads. Creo offers several constraints, including fixed support, displacement, cylindrical support, and planar support, allowing for a wide range of simulation scenarios. In addition, the option to add load case is used when the part is being optimized for multiple separate loads and constraints.

In Creo generative design, there are two optimization methods to choose from: stiffness and mass optimization. Stiffness optimization is recommended when controlling deformation is important, and it can be achieved by limiting the volume or weight of the generated design. On the other hand, mass optimization is a new feature in Creo 9 that minimizes mass for a given safety factor instead of optimizing for stiffness. This is a major improvement for cases where stiffness is not critical, simplifying the optimization process. The safety factor in mass optimization is dependent on the yield strength of the material, making it a more efficient approach in certain scenarios.

There are several design criteria to be considered, it is very important to define specific criteria depending on your design and desired results. The design criteria can be specified in terms of a set of constraints, such as maximum stress, minimum displacement, or maximum frequency response, as well as a set of objectives, such as minimizing weight or maximizing stiffness. In this case using Creo, the main design criteria available include constraints like build direction, critical angle, material spreading and minimum crease radius. The only way to manufacture such complicated geometry is 3D printing, and therefore defining a print direction is essential to keep in mind. Usually, this is directly linked to the critical angle, which if it is surpassed, will need support structures when printing.

Build direction refers to the direction in which the layers of material are deposited during the 3D printing process. This direction can have a significant impact on the properties of the final product. For example, if the build direction is perpendicular to the direction of applied stress, the part may be weaker and more prone to failure under load. On the other hand, if the build direction is parallel to the direction of applied stress, the part may be stronger and more resistant to failure.

Critical angle, also known as overhang angle, is the maximum angle at which an object can be printed without requiring additional support structures to prevent it from collapsing under its own weight. This angle is determined by the material properties of the 3D printing material, as well as the geometry of the object being printed. If the maximum overhang angle is exceeded, the printed object may sag or collapse, resulting in a defective or unusable part.

In many cases, one cannot avoid using support structures, but limiting their usage of them is desirable. Depending on the geometry, one will need to judge what direction is the most feasible to be physically printed, of course accounting for the always-present gravity. Observing where there are built overhangs will help determine what direction it will be easier to print without the need for support structures.

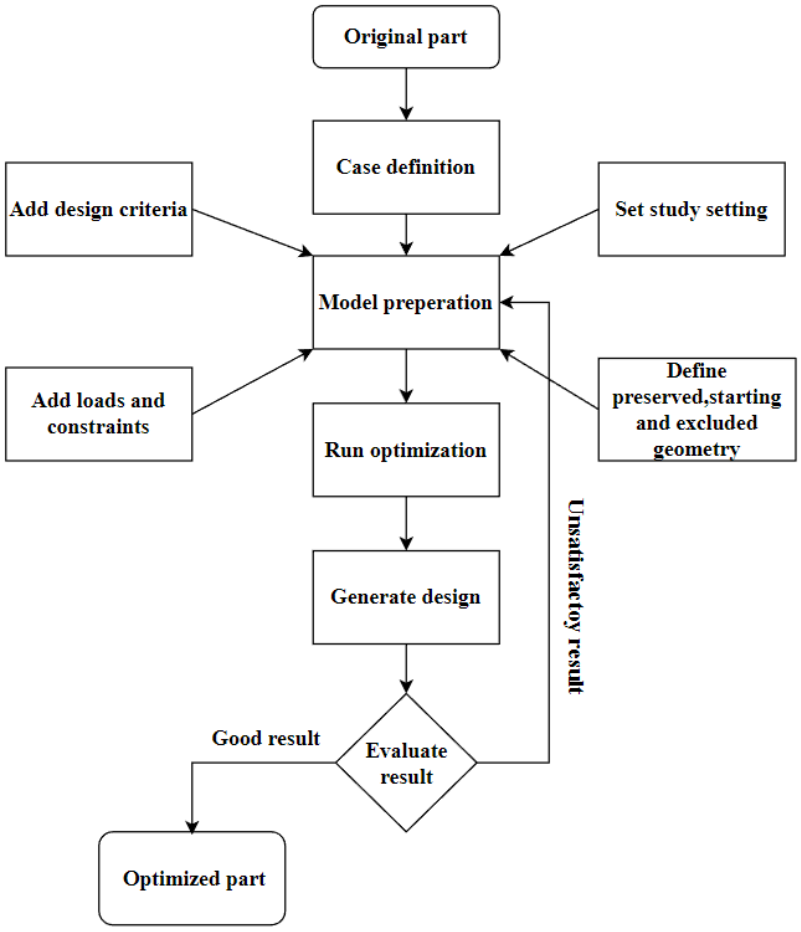

Figure 6 Flow chart of the optimization process

The generative design tool in Creo does include finite element analysis (FEA) results, however these results are only approximate. Therefore, an Ansys FEA is performed for the generated designs, where stresses and deformation are evaluated. Figure 6 shows a flow chart of the process described in this chapter.

3.2 Finite element method

FEA is a highly complex and intricate method that is utilized for solving some of the most challenging engineering problems. This computational technique can break down even the most complicated systems or structures into smaller, more manageable pieces - known as finite elements - which can then be analyzed to determine the behavior of the overall system. It uses highly advanced mathematical models being simulated using equations of physical properties, external loads and boundary conditions.

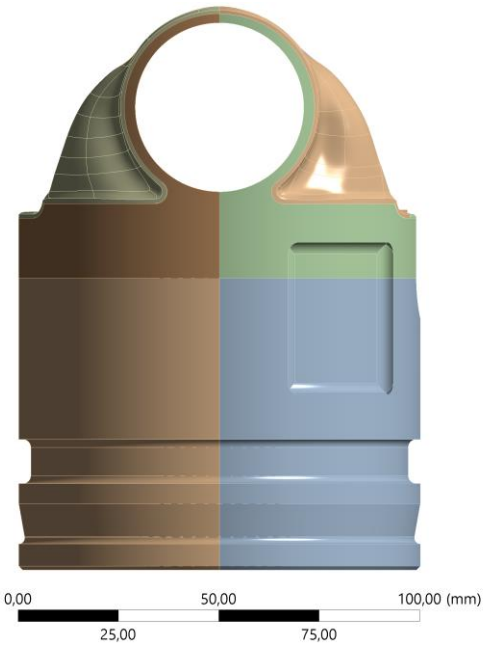

Figure 7 Example of a sliced part

In this thesis, FEA is used for simulating and calculating loads and stresses on both the original parts from BE and the new redesigned parts. It is done by converting the finished .prt file from Creo into a .stp file compatible with the FEA software. Most of the process is done in Ansys Mechanical, which is the FEA software within Ansys. In some cases, the geometry might be too complicated for Ansys to mesh. By slicing the part in DesignModeler, one usually counters this issue by reducing the number of elements in total by separating it into parts, as shown in Figure 7. When choosing mesh size, it is important to keep in mind that smaller mesh sizes produce more accurate results at the cost of processing time, and vice versa. After simulation results, a relatively common occurrence is the emergence of singularities. These are small points on the geometry where a high stress concentration occurs. This can usually be ignored as they are not real, stress is force divided by area and therefore the stresses at those small points are unrealistic. An example of FEA usage seen in Figure 8.

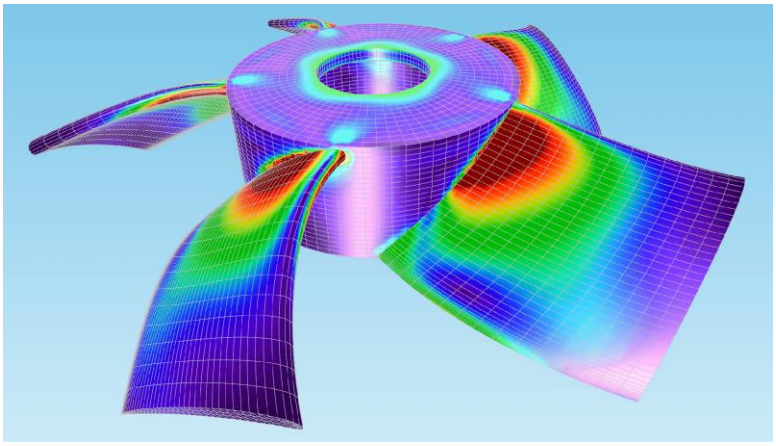

Figure 8 Illustration of a FE analysis [22]

3.3 Lattice

Another option to save material and weight in AM is by using lattice structures. They are mostly known in nature as cell structures such as in human bones and in honeycombs, but within manufacturing it is commonly known as the infill used in 3D printing. Using lattices as infill when printing is a way of saving material and time instead of printing a part fully solid. Different lattice structures have its own uses, strength and weaknesses as mentioned before, depending on its purpose.

In Creo one needs to define separate bodies, as the lattice function uses a body to generate lattice as infill with an outer shell or replace the entire body with lattices. Creo is not the most expansive software for lattices, as the options are limited. 2D cells are triangular, square, pentagonal and octagonal, while the 3D cells are simply octagonal and stochastic which are the most complicated lattices available in Creo. A problem with the 3D lattices is that the geometry often ends up quite computational expensive, making it hard to simulate. To overcome this, simplified lattices can be generated in Creo, allowing the lattice to be evaluated much faster than the full lattice geometry. The lattice dimensions can be changed in any direction and every element of it can be edited. The lattice density is uniform as standard, it is also possible to create lattices with variable density based on simulation results of the original part. A gyroid lattice is shown in Figure 9.

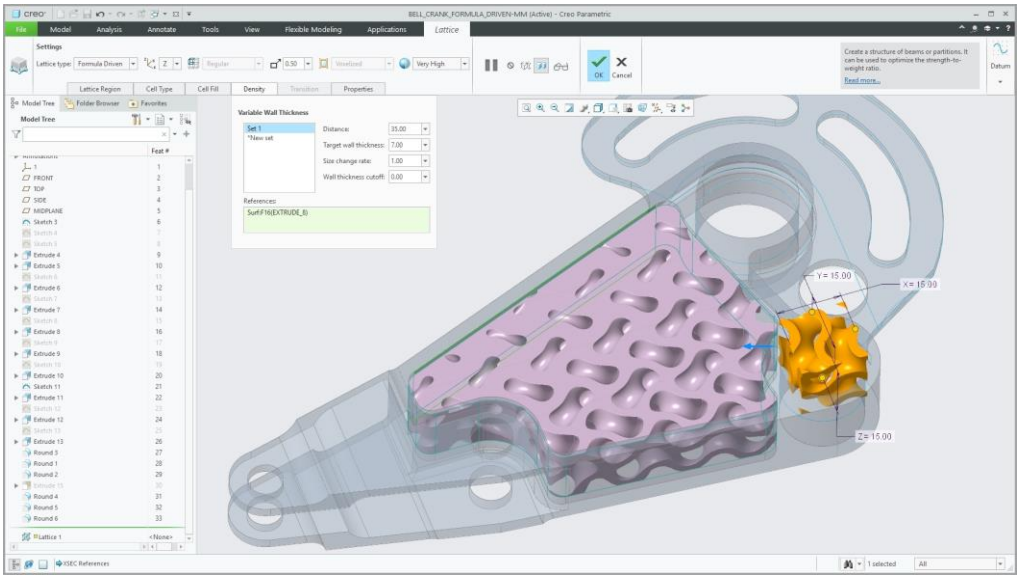

Figure 9 Example use of lattice in Creo [23]

4. Case studies

Bergen Engines have provided four cases, with each case having its own set of goals. The common goals for all cases are to reduce assemblies and weight. In this case study, strategies will be explored with an AM mindset to achieve these goals, while also satisfying the specified requirements for each case, such as forces, fatigue limit and safety factors.

BE gave most of the necessary data for the case study. This includes step files of the parts, loads, constraints, and a deformation limit of 10 +- % of the original parts. The safety factor was set based on the FEA results from ANSYS and calculated with this formula:

$$\text{Safety factor} = \frac{\sigma_y}{\sigma_{max}}$$

Where σ_y is the yield strength of the material and σ_{max} is the maximum stress from the simulation results.

4.1 Case 1 Lifting tool for turbocharger foot

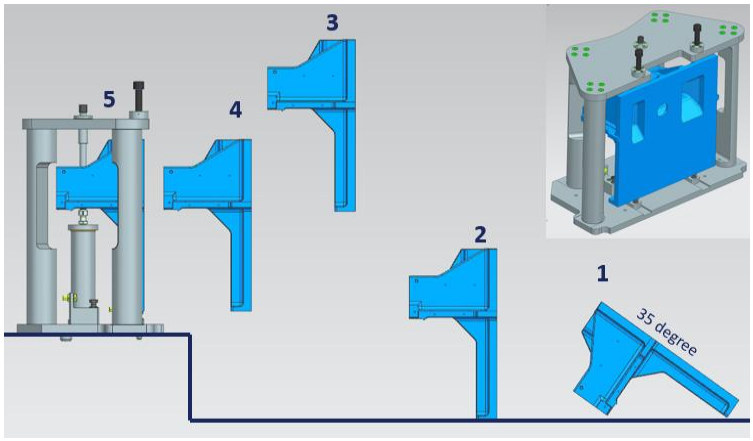

Figure 10 Lifting procedure for turbocharger foot

The lifting tool is used to lift the turbocharger foot into a fixture, where it is machined and lifted out again, this process is shown in Figure 10. The goal for this case is to create a new design for the lifting tool with a pure AM mindset. The turbocharger foot currently requires a complex lifting tool, with several moving parts to be lifted. Bergen Engines did not provide any original part for this case, only the turbocharger foot and the fixture to where the foot is placed to be machined.

The tool is A safety factor of a minimum of 2 is required for the tool and the 300 kg turbo charger foot is the only applied load. The lifting tool has three main constraints. Constrained by the steps given in Figure 10, it must not come in contact with the fixture and be light enough to be handled by one person. It is also important that the lifting tool is user friendly without much complexity. Another factor to consider is to make sure the production of the part does not get too costly. BE did not want the original lifting tool to affect the AM design, which is why it was not given. With a pure AM mindset, part complexity is not an issue. This can eliminate the need for assemblies and weight can be reduced to a minimum by performing topology optimization.

4.2 Case 2 Nozzle holder housing

The nozzle holder housing shown in Figure 11, is an important part of the fuel injection system. This is a heavy part that also needs cooling due to the heat from the combustion chamber. The goal for this case is mainly to minimize the weight. Only a static load is applied to this part, it is fixed at the top with two bolts.

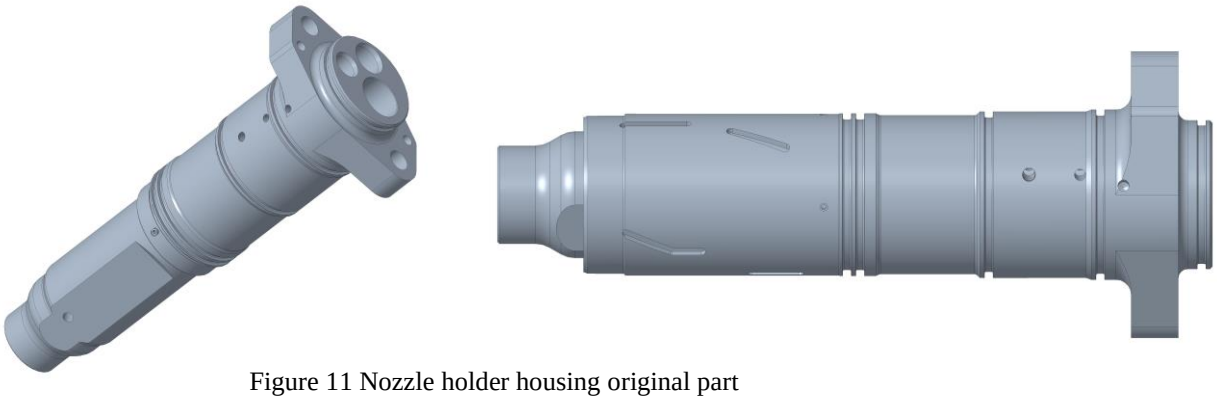

Figure 11 Nozzle holder housing original part

The nozzle holder housing is a heavy and solid part with a low relative load. This provides great potential for weight reduction. Although there is a lot of material that can be removed, most of the machined features must be preserved in the optimized part, making optimization more difficult.

The bolt loads are simulated by applying a 43000 N force around the holes. Due to missing information regarding boundary conditions, it was assumed and placed at the bottom with fixed support, boundary condition and loads are shown in Figure 12.

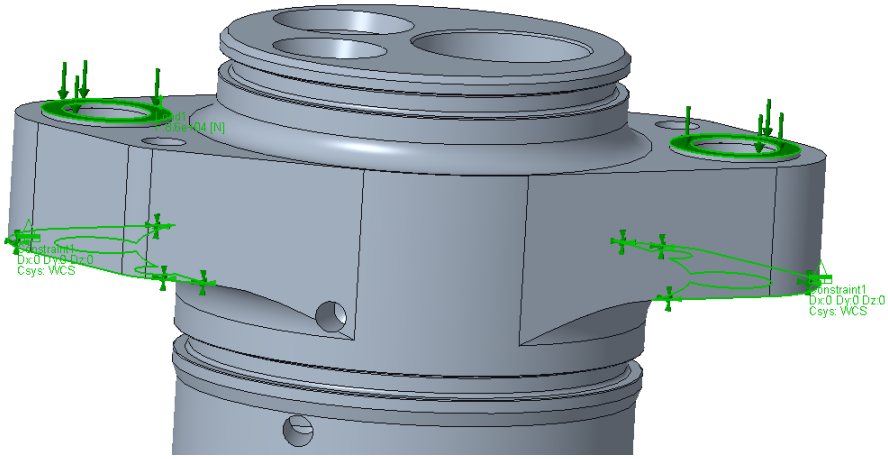

Figure 12 Nozzle holder housing, load and constraint highlighted in green

4.3 Case 3: Injection cam follower

Figure 13 Injection cam follower, Original part

The injection cam follower, shown in Figure 13, is a part of the fuel injection system, and it is driven by a camshaft. The load from the camshaft causes high cycle fatigue and leads to a stress concentration in the rounded corners, eventually causing cracks to form. Real-life model is shown in Figure 14. This part must be lightweight and is therefore produced in aluminum alloy. The goal is to optimize the design and weight of the injection cam follower for steel, without increasing the parts weight. Steel is much stronger and will prevent cracks from forming.

Figure 14 The real-life model with the strained areas visible

When opting for reducing weight, there are a few different options in this case. The loads and stresses in this part are located mainly in the lower half, where the part is the most solid. The cylinder walls are also areas where mass can be reduced since there will not be any major loads there. Because there are

several factors such as cut-outs, oil flow and channels that need a workaround, the percentage of mass reduction is limited. In theory, it should be possible to minimize mass to around 30-35% of the original, meaning just enough for it to be replaced by aluminum.

Loads and boundary conditions

The camshaft applies 63000 N force to the cam roller at an angle. This angle is assumed to be maximum 40 degrees. Figure 15 shows the load is applied to the inside surfaces of the shaft holes. To simulate 40 degrees, the angular force was decomposed into a horizontal force of 40478 N and a vertical force of 48275. Figure 16 shows that fixed support is assigned on top of the inside platform.

Figure 15 Injection cam follower Applied force

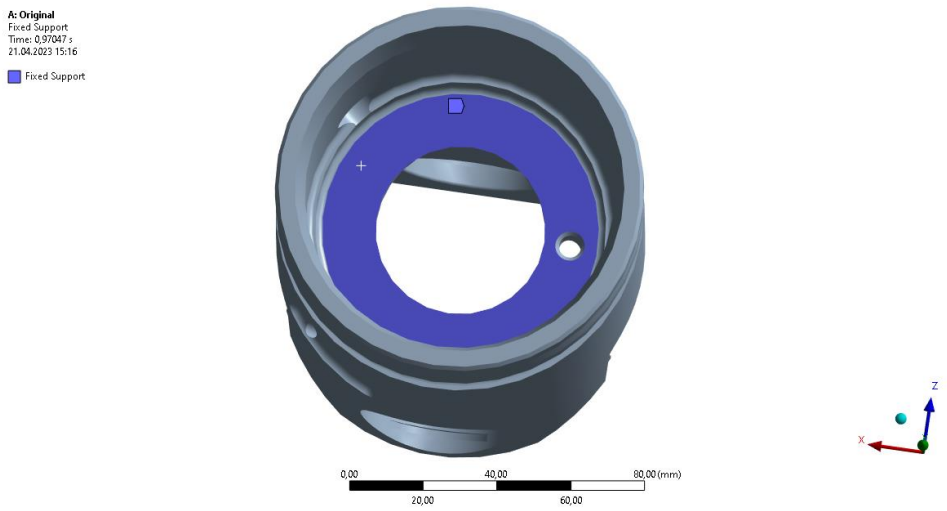

Figure 16 Injection cam follower Fixed support placement

4.4 Case 4: Valve bridge

The valve bridge shown in Figure 17, is an important part of the opening and closing of the exhaust valves. A rocker arm applies a load on the middle “head” of the valve bridge. The two arms then push down the exhaust valves, opening them. To make sure the valves always open at the same time, one side of the valve bridge is adjustable to accommodate for uneven wear. The valve bridge consists of four parts that must be assembled. Good fatigue properties are required due to a high cyclic load. In addition, the head that receives load is hardened to avoid cracks. The goals for case 4 are to decrease the weight, minimize assembly, maintain a hardenable head and stiffness of the part.

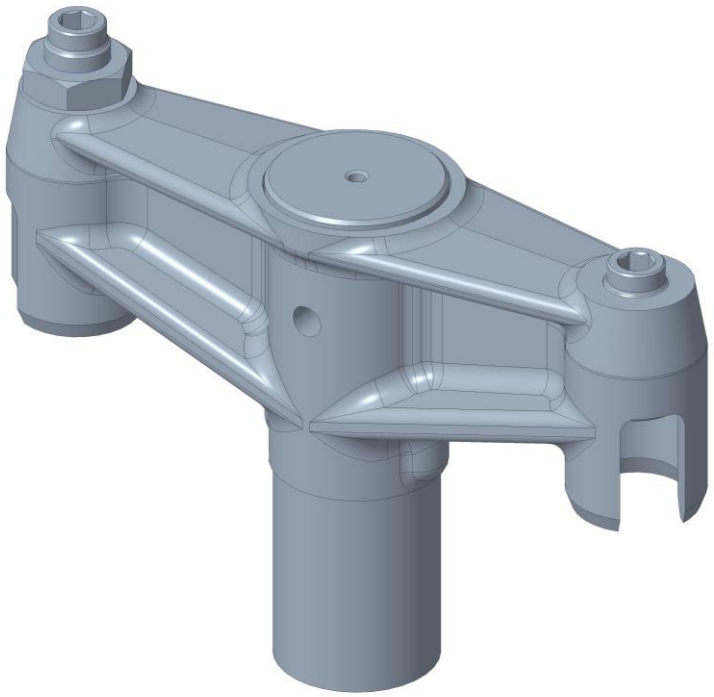

Figure 17 Original valve bridge

The valve bridge is a simple part with few features compared to cases 2 and 3. This means that there is a lot of mass that can be removed without losing any of the functionality. Consolidating the assemblies can also have a positive impact on the weight.

Loads and boundary conditions

Two load cases were considered for the simulation. In the first load case, the force would be placed on top of the middle head and constrained the part on both sides, with fixed support placed on the flat surface under each arm, where the exhaust valves would contact the valve bridge. The purpose of the second load case shown in Figure 18 andFigure 19, was to achieve more realistic deformation and load, as the arms were no longer fixed. This was considered the best load case and was therefore chosen. The oil pressure in the oil channel is very low and could be neglected. The maximum applied load is 35260 N.

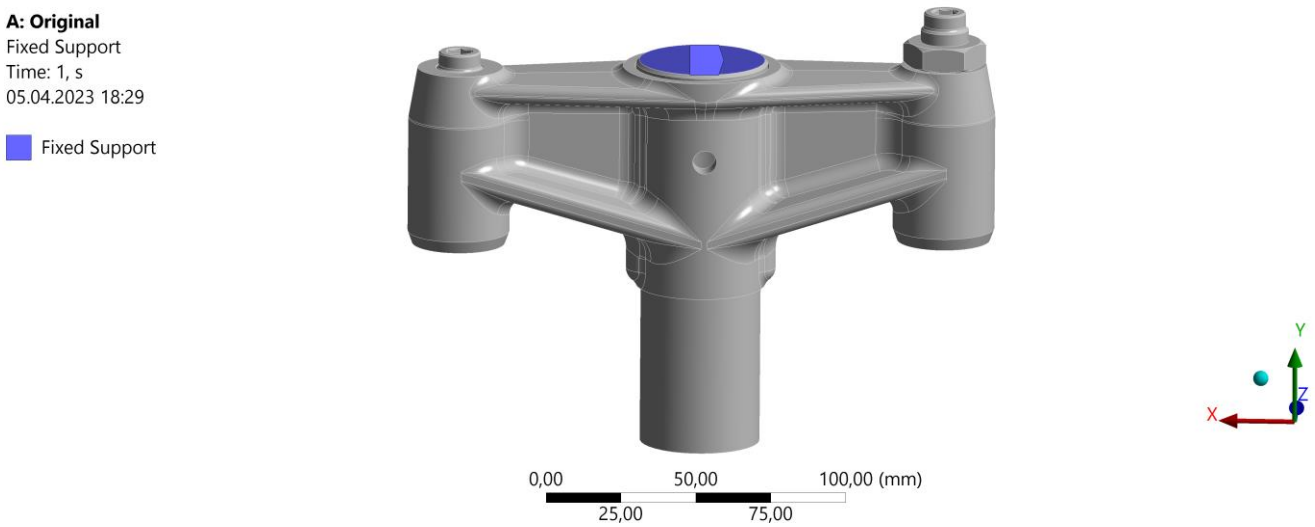

Figure 18 Valve bridge Fixed support

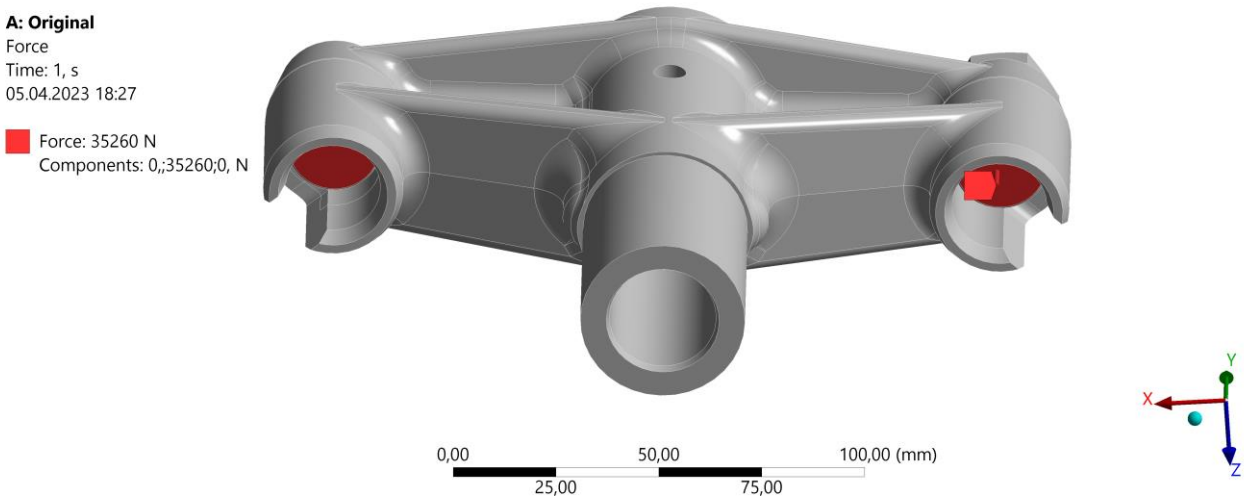

Figure 19 Valve bridge Load

5. Case study results

This chapter shows the design process and the design results of the case studies. Weight, stresses and deformation results are also presented. A comparison between the original parts and the new optimized will be discussed. All estimated costs are done with Amotools and are without post processing.

5.1 Case 1 Lifting tool for turbocharger foot

5.1.1 Design

Topology optimization was used to create the new design. Safety and functionality were two important factors considered. The lifting tool had to be stable enough to ensure a safe lifting operation, while also leveling the foot so that it would fit in the fixture. Aluminum alloy was considered a good material choice as it is very lightweight and strong enough for the application. Parts in both 316L steel and titanium alloy are also included. Two designs are created, one more advanced preventing the rotation as mentioned and providing added stability, and one simpler design with weight saving in focus.

Design 1

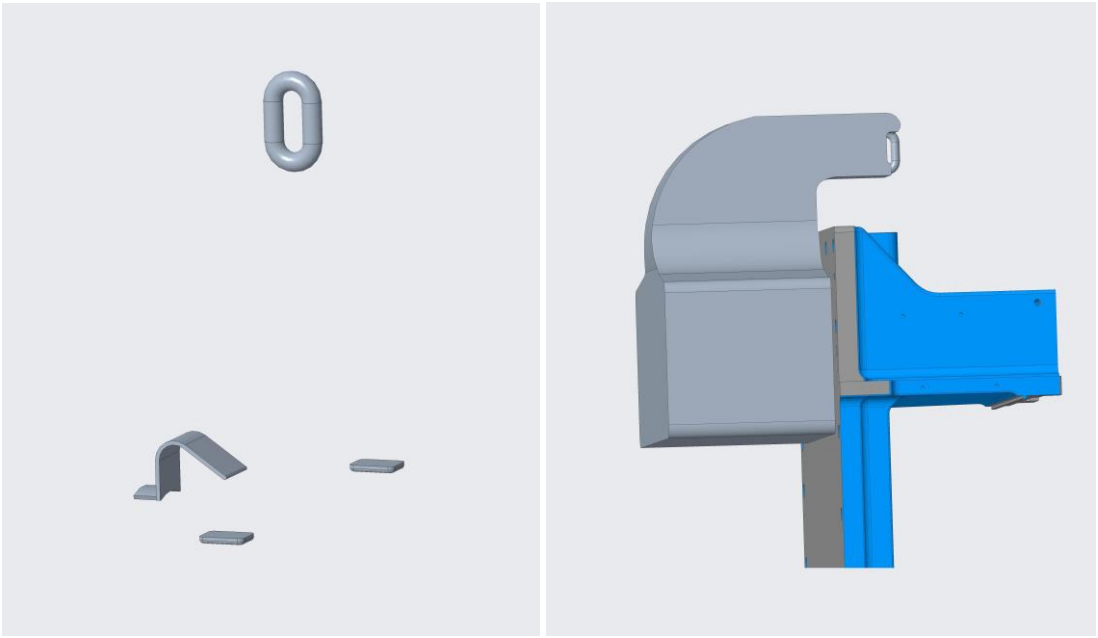

Figure 20 Lifting tool, preserved bodies to the left, starting geometry to the right

In Figure 20, the preserved bodies consist of a central hinge, two equal support pads and an eye hook at the top. The eye hook is located directly above the center of gravity of the foot in its upright position. The two pads support the weight of the foot and provide stability. Because the foot is initially laying down, the tool utilizes a second eye hook to grip the foot. This will initially support most of the weight during the lift and then gradually decrease as the foot rotates to an upright position, distributing the load to the support pads as well. The central hinge is also important for safety, as it prevents the foot from sliding off the lifting tool. The starting geometry is a large box with a bottleneck shape to prevent the material from spreading too far. It is also shaped to prevent contact with the fixture.

Two load cases were defined. The first case is when the foot is laying on the ground and will be lifted. A force of 2948 N is applied to the surface of the central hook downwards at 35 degrees. A fixed constraint is placed at the top hook for both cases. Once the foot is lifted off the ground, the second load case is defined, where the same force is applied to both the middle hook and the support pads. Build direction is set to be from left to right in reference to the figures below, as this is found to require the

least support structures. The mass limit is set to 3kg. The optimization method used is to maximize stiffness, as it is the most important factor and Creo was not able to successfully optimize for mass.

Design 2

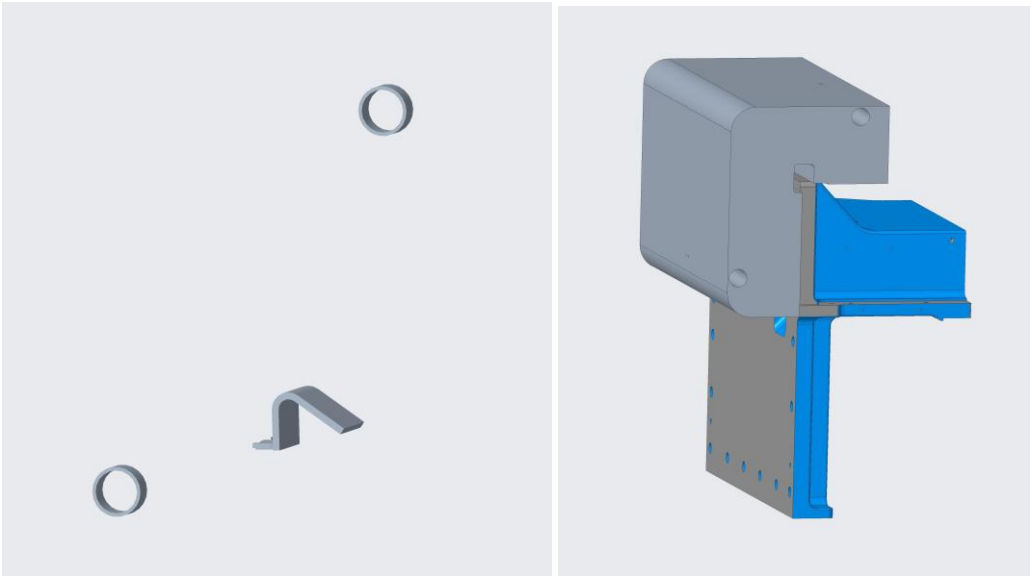

Figure 21 Lifting tool, Preserved bodies to the left, starting geometry to the right

Design 2 is similar to design 1, the main difference being the lack of support pads and the addition of an eye hook at the bottom, shown in Figure 21. One main goal of this version is to enable lifting from two eye hooks, providing enhanced stability during the initial lift, and performing the rotation of the part once it is raised above the ground. Design 2 also has two load cases. The first case with fixed support applied to both eye hooks and a downward force of 2948 N at 35 degrees, applied to the hinge. For the second case, only the top eye hook is fixed, and the same force is applied vertically.

The surface of the hinge is shaped after the curves inside the hole of the foot, where the hook would fit as can be seen in Figure 22. It is also designed to fit before and after the machining of the turbocharger foot.

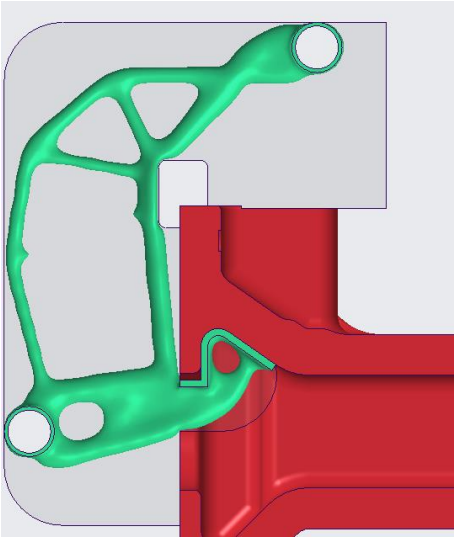

Figure 22 Lifting tool Hinge design

Both designs were 3d printed in plastic (PLA) using fused deposition modeling at 25% scale with HVL's Ultimaker 2+ Connect, to test functionality. This proved to be very useful as it revealed how well the designs worked and the improvements that could be made.

5.1.2 Results

The part never made it into Ansys, as the reconstruction failed consistently. Therefore, the simulation results had to rely on the analysis from Creo.

Design 2 316L

After printing this part with PLA, this design was found to work fine by picking the foot up and lifting it normally straight up. Its main weakness was when simulating lateral movement, it lacked a bit of stability. The foot would get a bit of a rotational movement if rotated or moved horizontally quickly enough, with the lifting tool having only one support hook in the middle shown in Figure 23. It also tended to tilt forward a bit while suspended, suggesting a small support beneath might be needed to compensate.

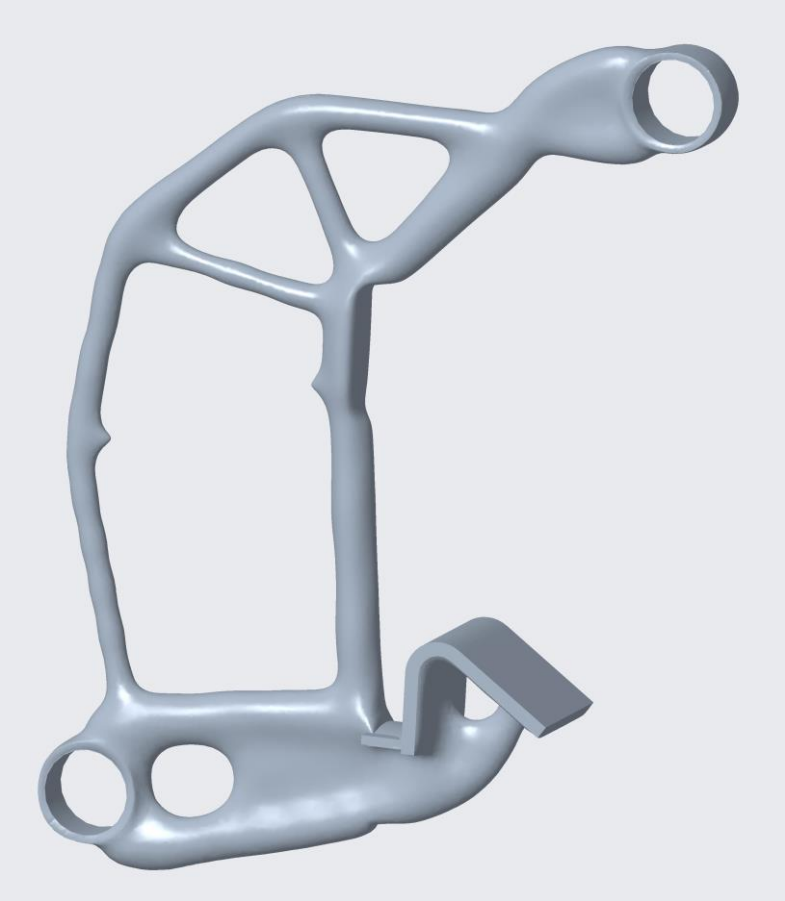

Figure 23 Lifting tool Design 2 316L

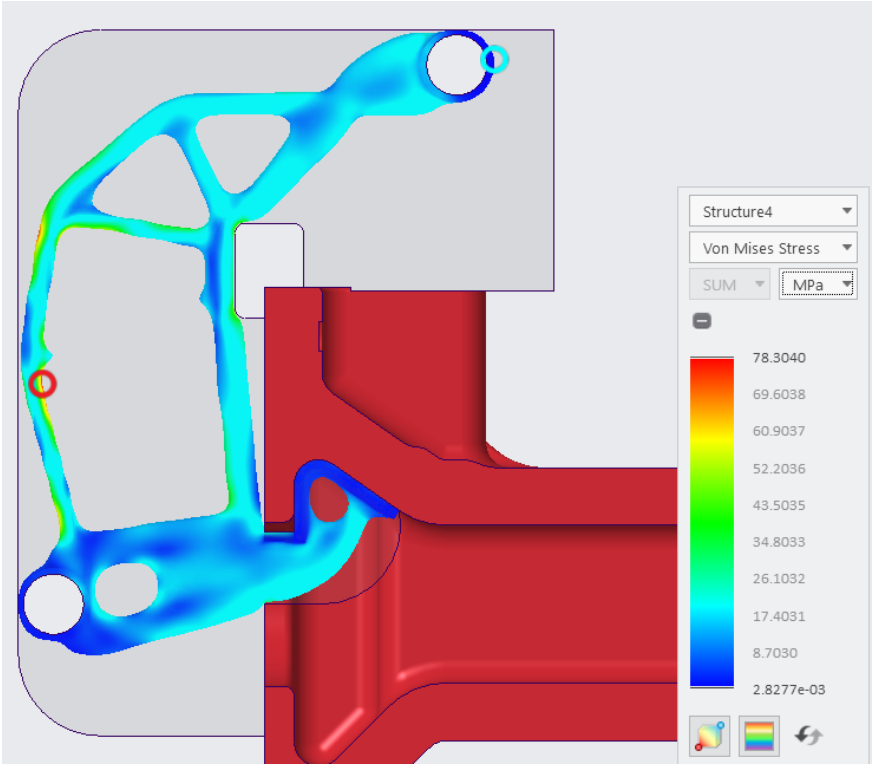

Figure 24 Lifting tool Design 2 316L von Mises stress

The highest stress in this design reached only 78 MPa, shown in Figure 24. The safety factor for this part is 6,2. According to Amotools.com the production cost of this design in 316L was estimated to be 2149€. Deformation was a decent 0,3 mm as shown in Figure 25.

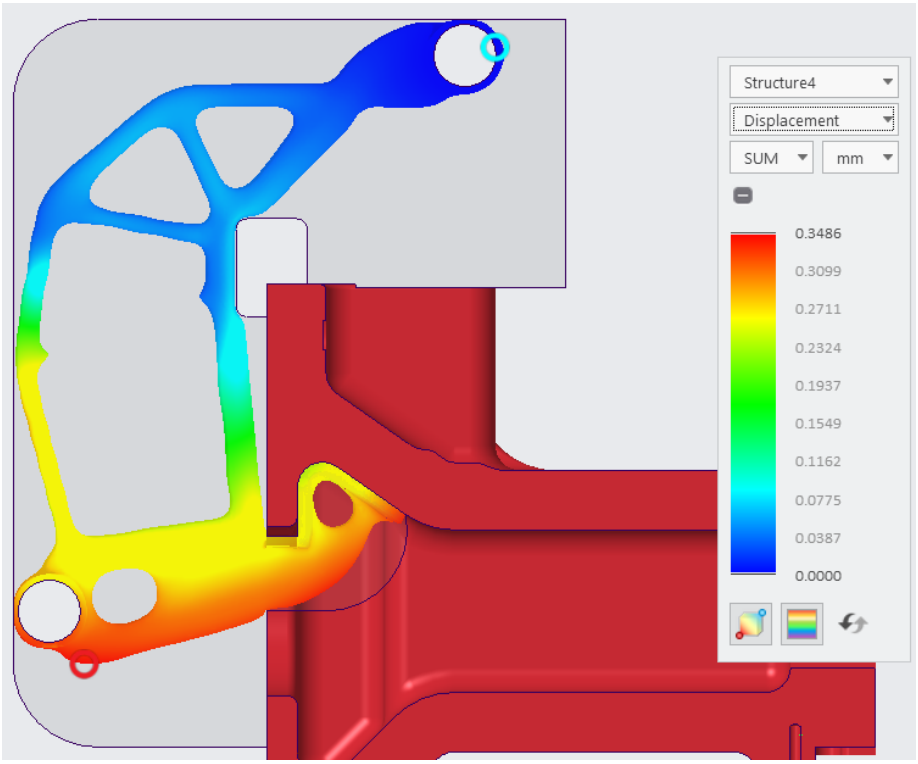

Figure 25 Lifting tool Design 2 316L Max deformation

Design 2 Ti-Al6-4V

It was also experimented with titanium to see how different the design and stresses would turn out. Notice how the titanium version in Figure 26 looks nearly identical to the steel version in Figure 24Figure 26 and therefore has about half the weight. The stress is also lower than steel at 54 MPa, and the deformation is nearly identical as seen in Figure 27. Amotools estimates the production costs of this in titanium to be 3346€. The safety factor for the titanium part is 17,3.

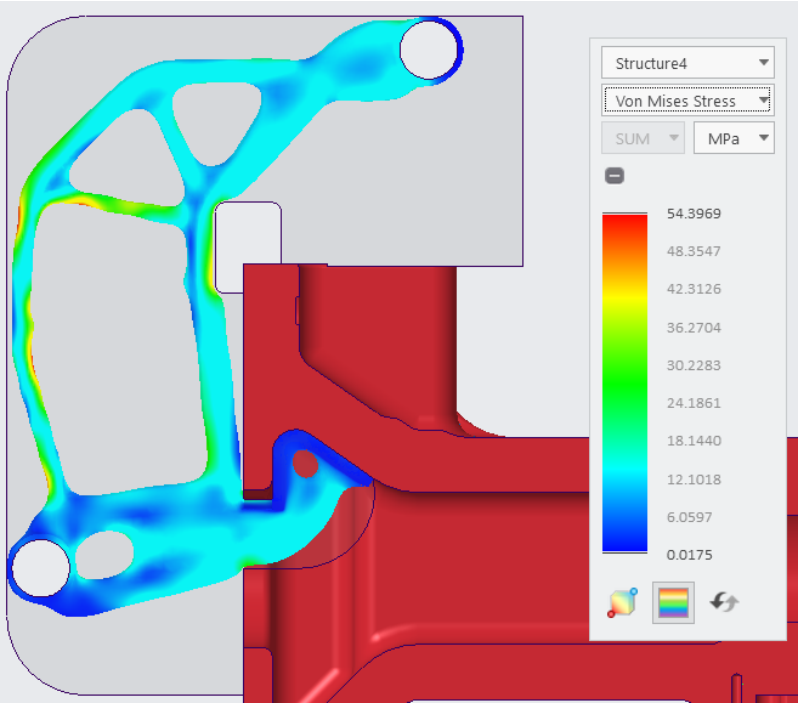

Figure 26 Lifting tool Design 2 Ti-Al6-4V von Mises stress

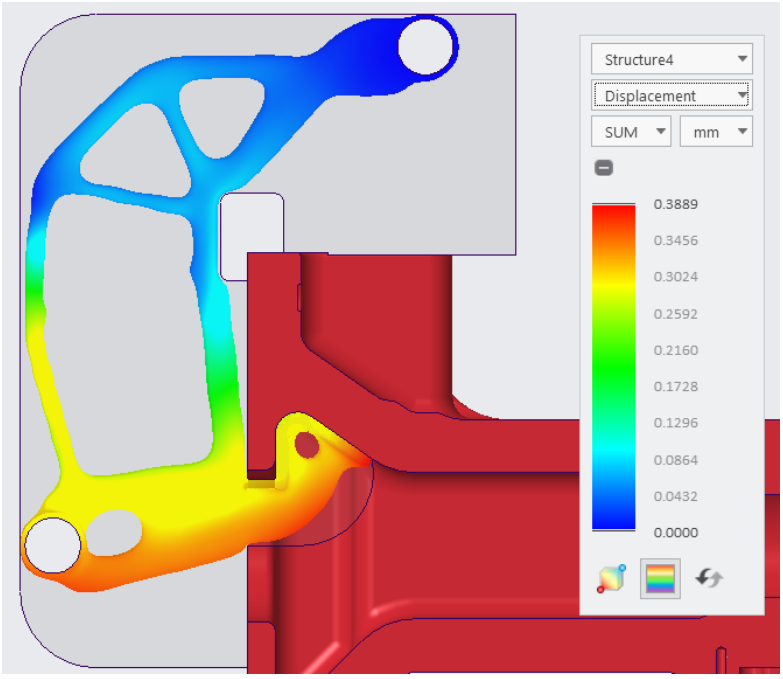

Figure 27 Lifting tool Design 2 Ti-Al6-4V Max deformation

Design 2 AlSiMg10

This same design was also optimized with AlSi10Mg, which showed even better results. The max stress was almost as low as the titanium shown in Figure 28, and the deformation only a 0,5mm difference in Figure 29. The weight resulted in only 1,1kg with a safety factor of 10,6. According to Amotools the production cost without post processing is estimated to be 1846€.

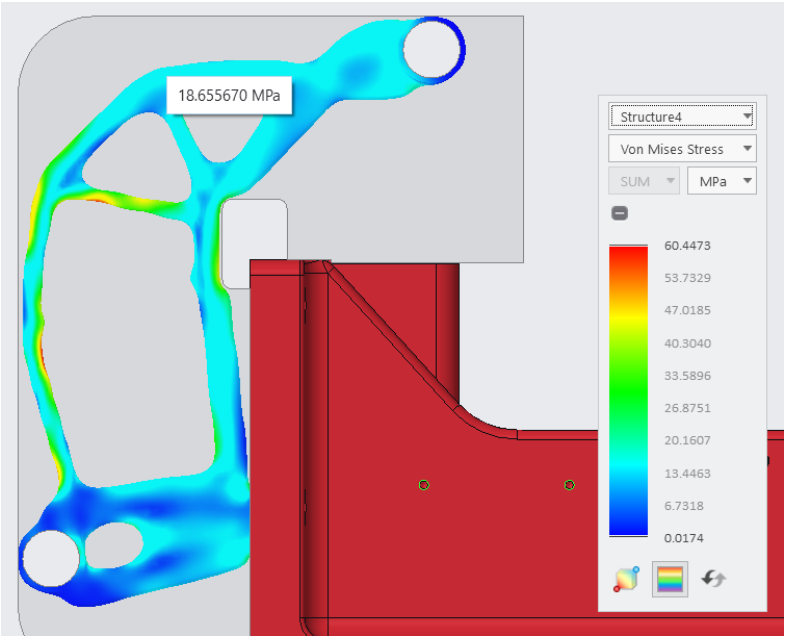

Figure 28 Lifting tool Design 2 AlSi10Mg von Mises stress

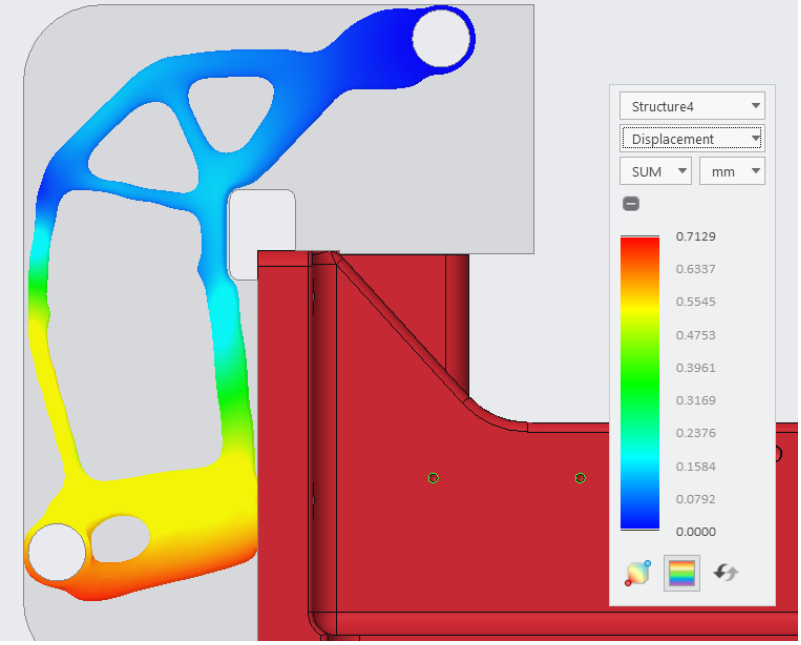

Figure 29 Lifting tool Design 2 AlSi10Mg Max deformation

To compensate for the lower stability where it tilts forward, an additional simple support structure seen in Figure 30 was made to prevent the tilting and keep it stable. This worked perfectly and the part was now much more stable both when picking and lifting the foot from the ground and moving it in the air.

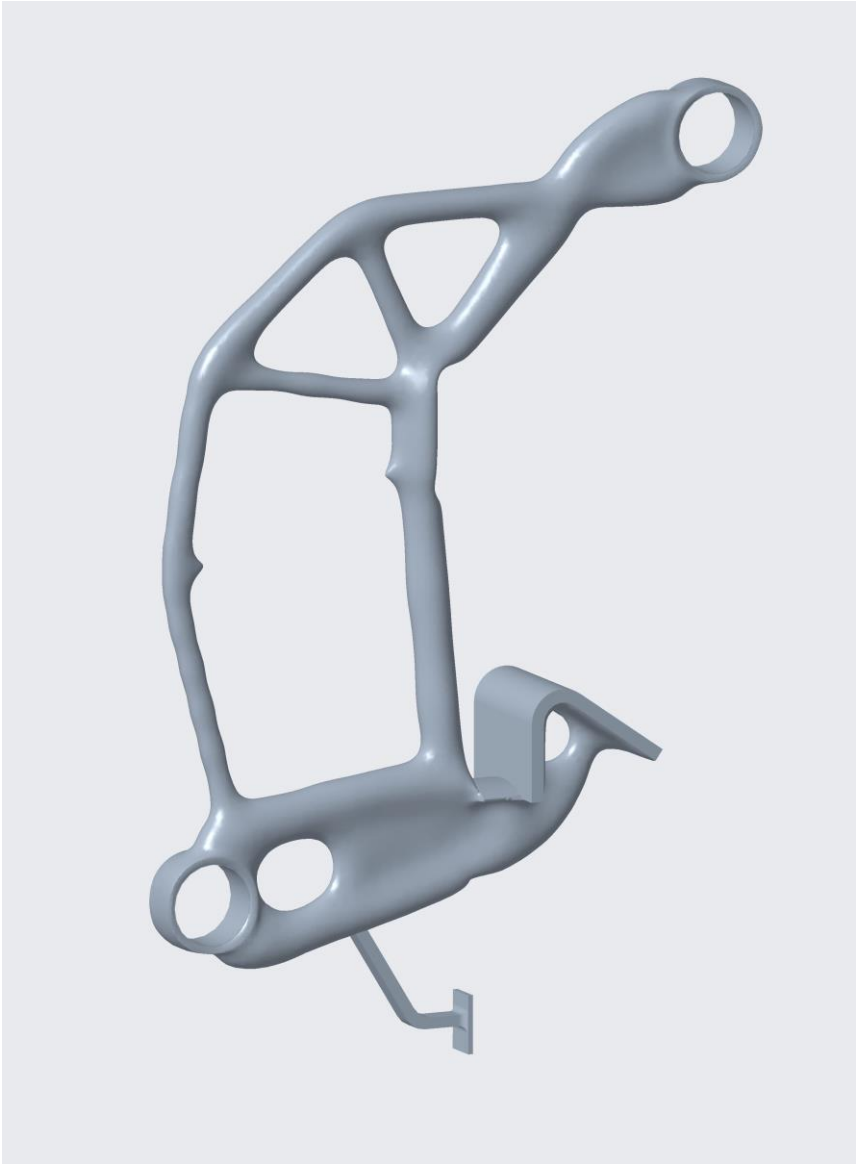

Figure 30 Stability support added to Lifting tool design 2 AlSi10Mg

Design 1

With added supports on each side, the lateral and vertical movements became more stable. Using AlSi10Mg for the optimization, it generated a structure of 2,5kg capable of lifting the 300kg foot with a max stress at 118,25 MPa shown in Figure 32. This is showing the loads from lifting the foot while on the ground at a 35-degree angle. The highest loads are concentrated at the top hook while the rest of the structure has relatively even and low stress values. These values over 118 MPa are so densely concentrated, they are assumed being singularities in this case. Figure 31 shows the first successful generated design of the design 1.

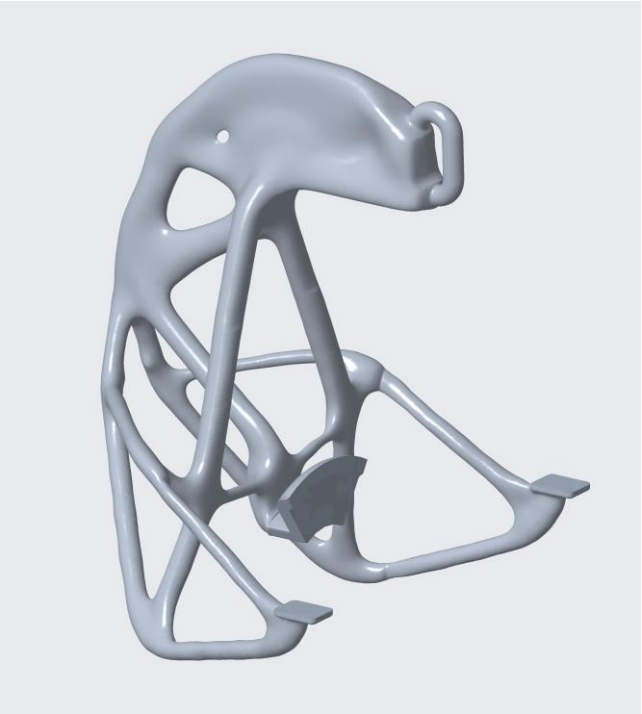

Figure 31 Lifting tool Design 1 AlSi10Mg

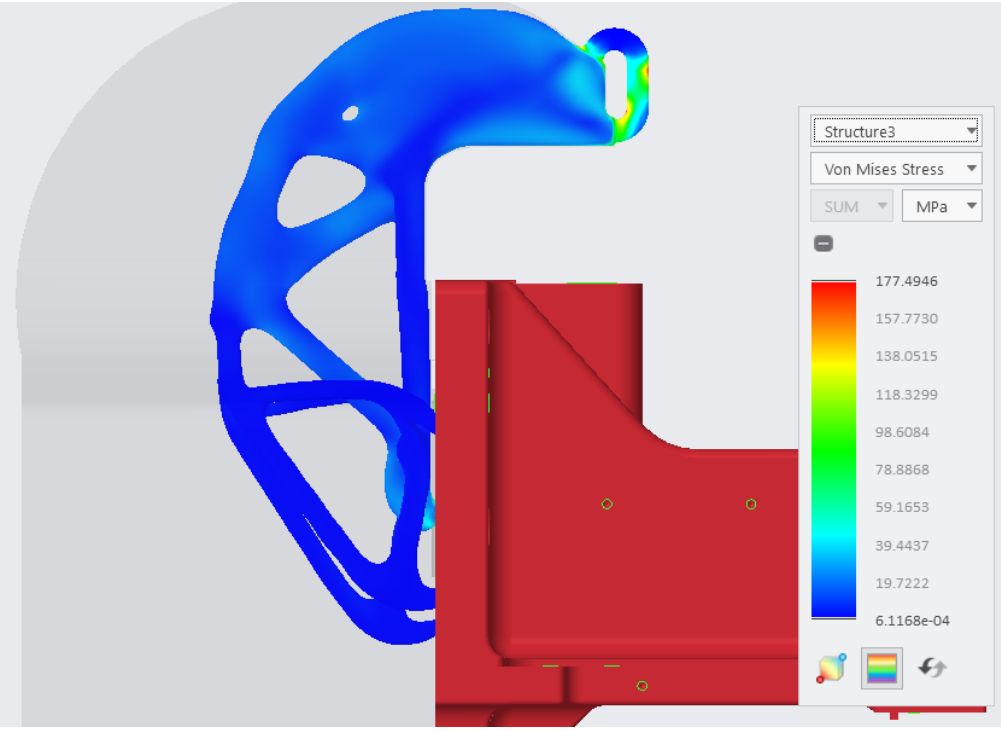

Figure 32 Lifting tool Design 1 AlSi10Mg von Mises stress

In the second load case the foot has been lifted completely of the ground and the forces are working vertically on the structure. Now the stresses are more distributed but also a lot lower overall with the highest stress at 41,5 MPa at a small, focused point shown in Figure 33. Deformation was slightly higher at 1,9mm shown in Figure 34.

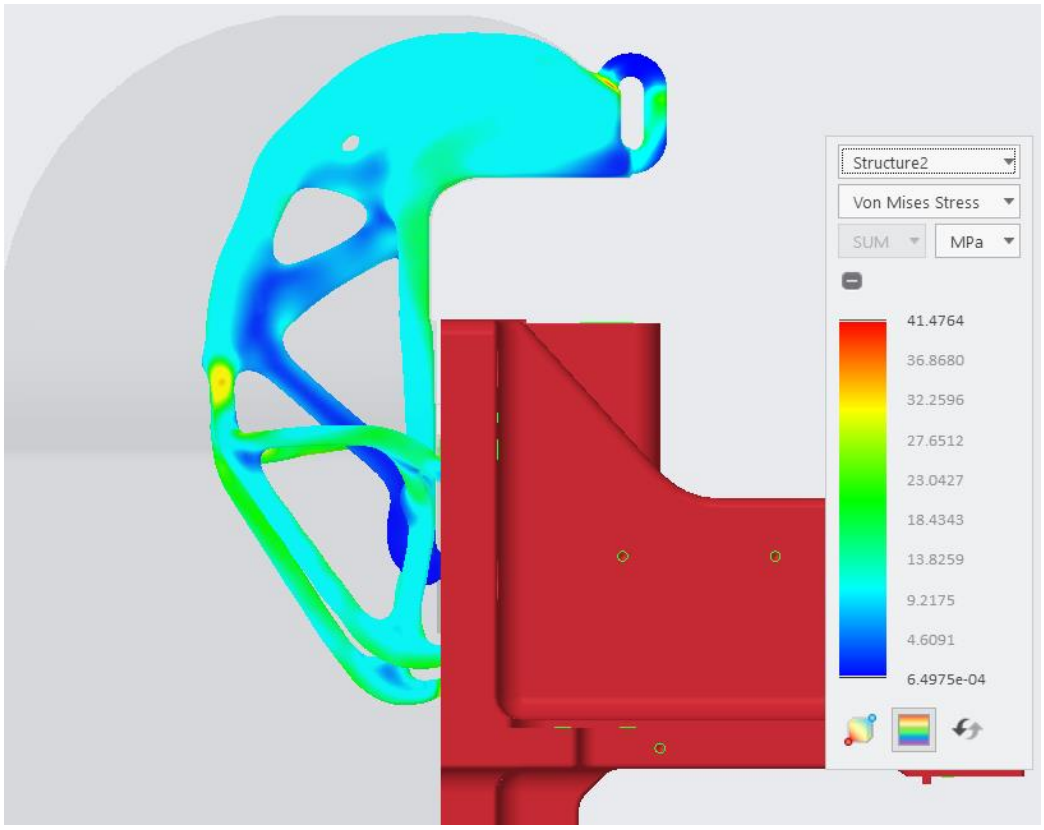

Figure 33 Lifting tool design 1 AlSi10Mg von Mises stress

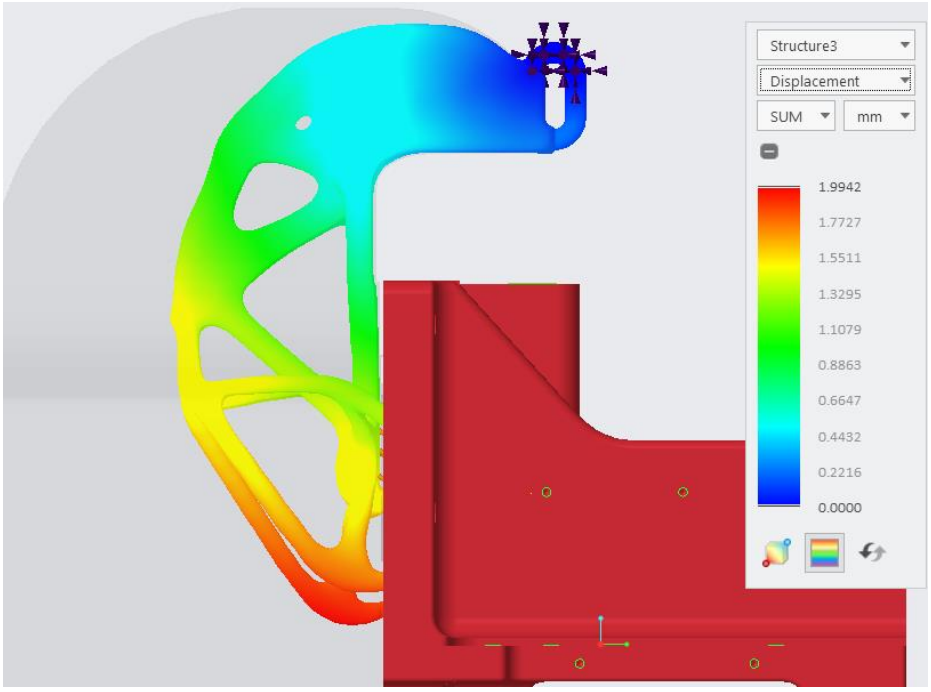

Figure 34 Lifting tool Design 1 AlSi10Mg Maximum deformation

Design 1 Improved

Despite the overall design 1 providing better stability, the hinge design shown in Figure 35 falls short of perfection. When lifting the foot from the ground, it was discovered that the hinge was sliding a bit in the hole and some lack of sturdiness in its grip. This is what the hinge in design 2 did better, therefore a version of design 1 with a better hinge was created. This was a combination of the best from both designs, taking the hinge design from design 2 and implementing it into design 1.

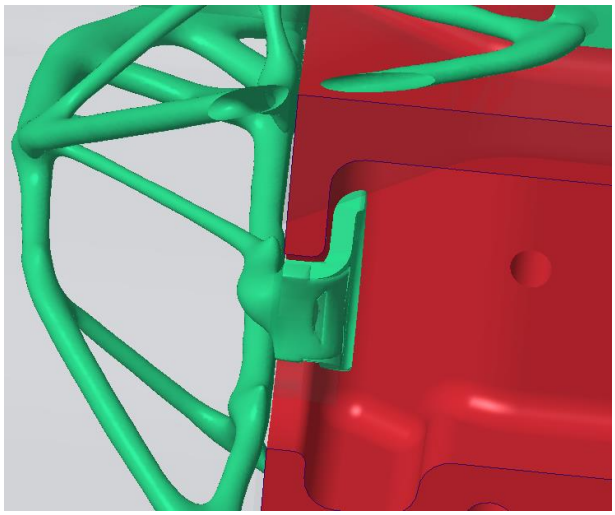

Figure 35 Initial hinge, Lifting tool design 1

A small change in the starting geometry was also made at the top of the eye hook, where stress was previously concentrated. This turned out to make a huge difference as opposed to the first version, where the highest stress had been reduced by approximately 90 MPa. The new and improved design can be seen in Figure 36.

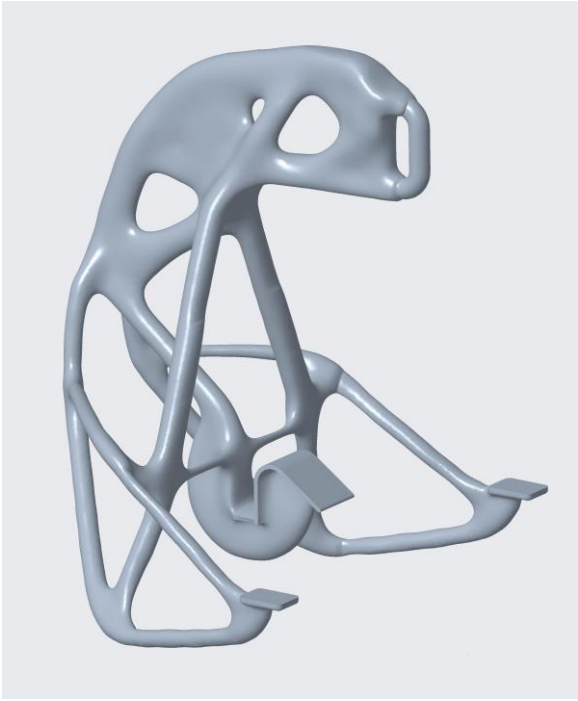

Figure 36 Lifting tool Design 1 AlSi10Mg, improved version

This design was made in AlSi10Mg, weighing 2,5 kg as well. It makes the part very manageable to handle by one person. The deformation is also improved as it is reduced to 1,3 mm shown in Figure 38, and Figure 37 shows that the maximum stress peaked at just 50 MPa while lifting from the ground. Maximum von mises stress when in the air ended up at 74 MPa shown in Figure 39, while the maximum deformation stopped at only 1 mm in Figure 40. By putting it into Creo assembly with the fixture, it is made sure it does not touch the fixture when placing the foot into it. The safety factor needed to be at least 2, and this design ensures a safety factor of 4,7. Amotools estimates part in aluminum cost at 3237€.

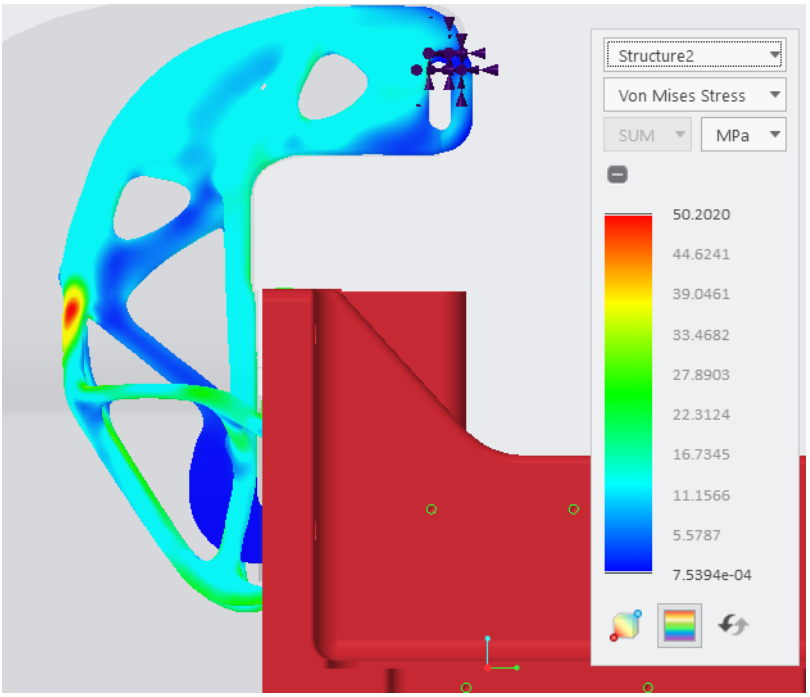

Figure 37 Lifting tool Design 1 improved AlSi10Mg von Mises stress, load case 1

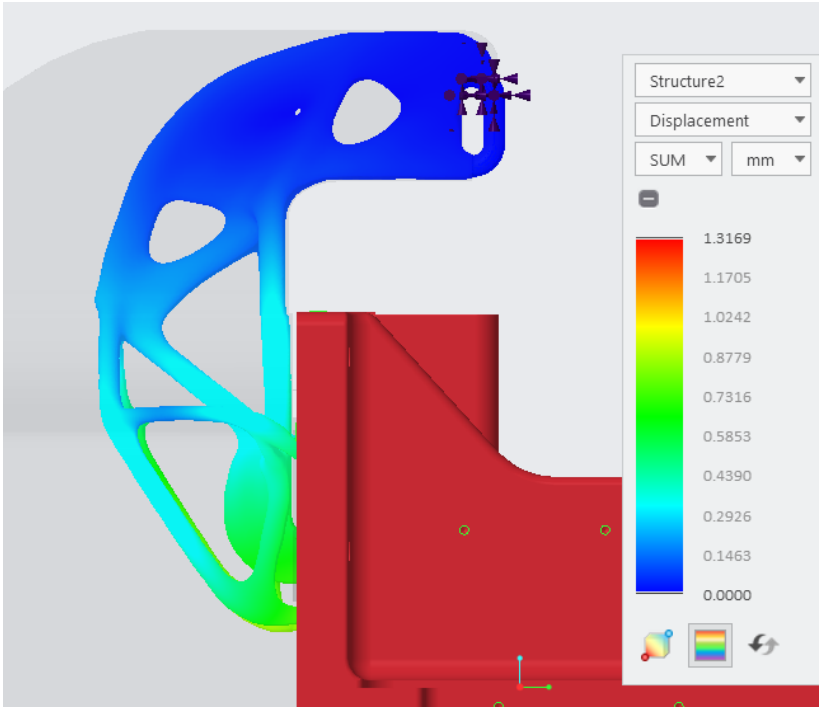

Figure 38 Lifting tool Design 1 improved AlSi10Mg Maximum deformation, load case 1

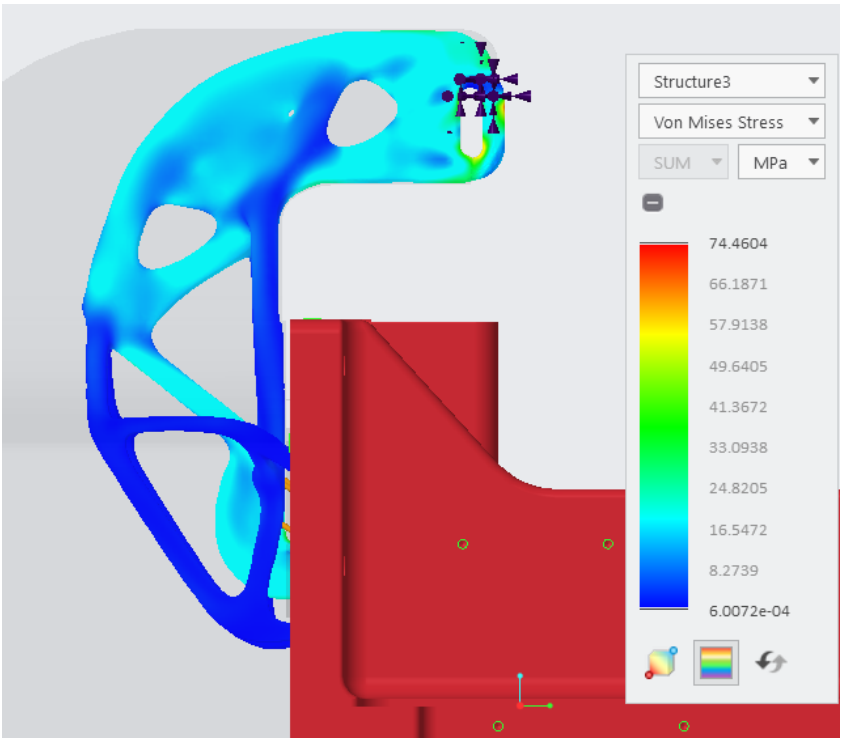

Figure 39 Lifting tool Design 1 AlSi10Mg improved von Mises stress, load case 2

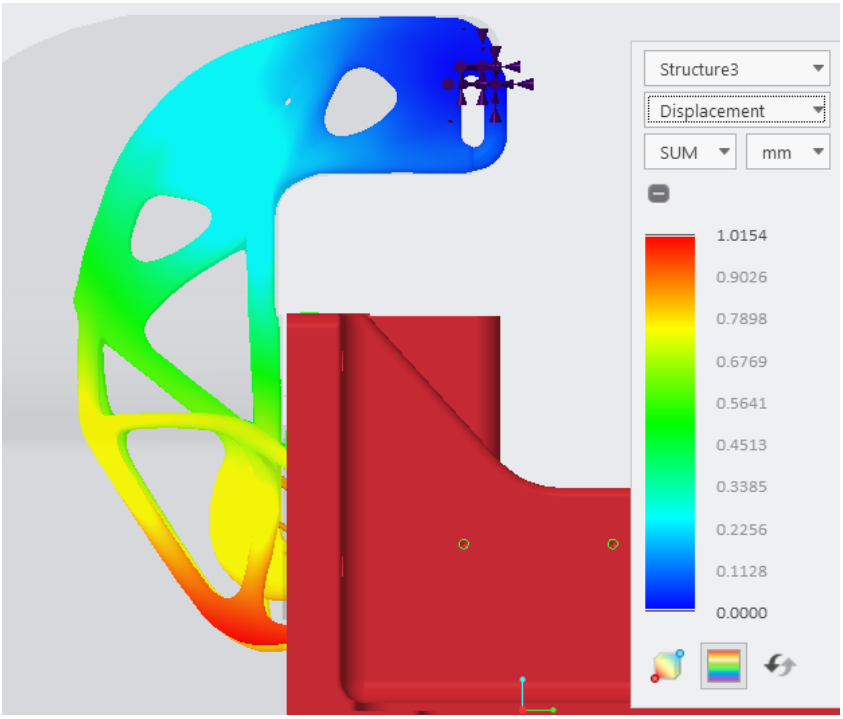

Figure 40 Lifting tool Design 1 improved Maximum deformation, load case 2

Design 2 attempt with 316L and Ti-Al6-4V

Making this version in 316L was also attempted but did not end up as a viable option. This was because when optimizing it, it always turned out too thin without connecting the bodies properly. Several settings were adjusted, among material spreading but without success as shown in Figure 41. This failed result was consistent. This was viewed as futile as getting a realistic functional part would end up weighing more than a similar version in other materials with similar performance and functionality.

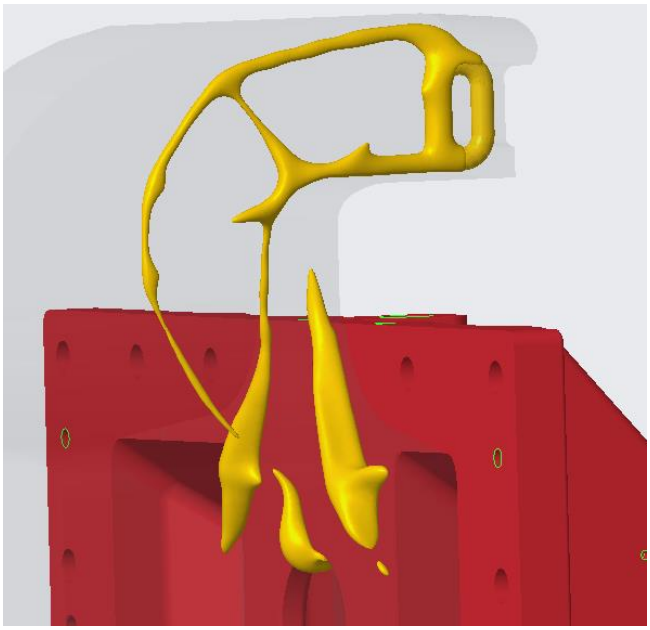

Figure 41 Lifting tool Design 1 improved unsuccessful with 316L

A similar case happened when trying to use titanium alloy, optimization was done both with and without material spreading, the result always ended up too thin, and not completely connected. To get a usable result, the weight limit had to be increased, and when it finally generated a result with analysis as shown below in Figure 42 and Figure 43, it ended up being 3,5kg with the safety factor at 10,22.

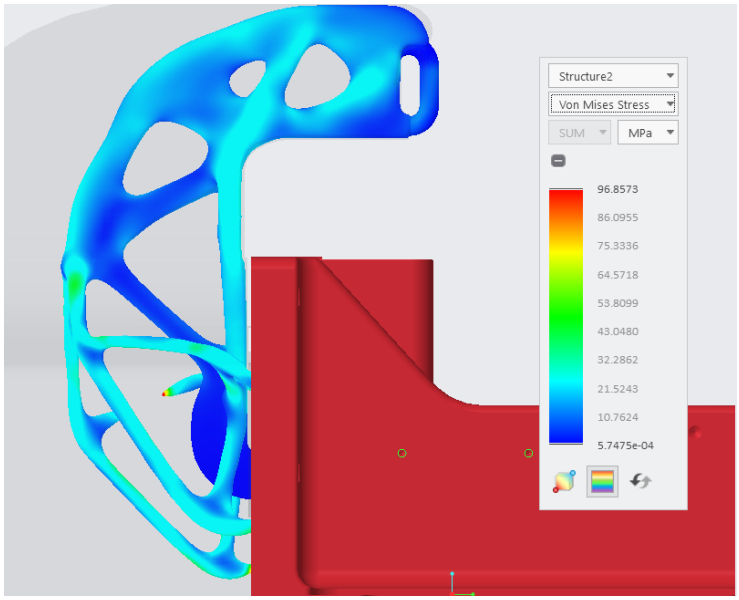

Figure 42 Lifting tool Design 1 improved TiAl4V von Mises stress

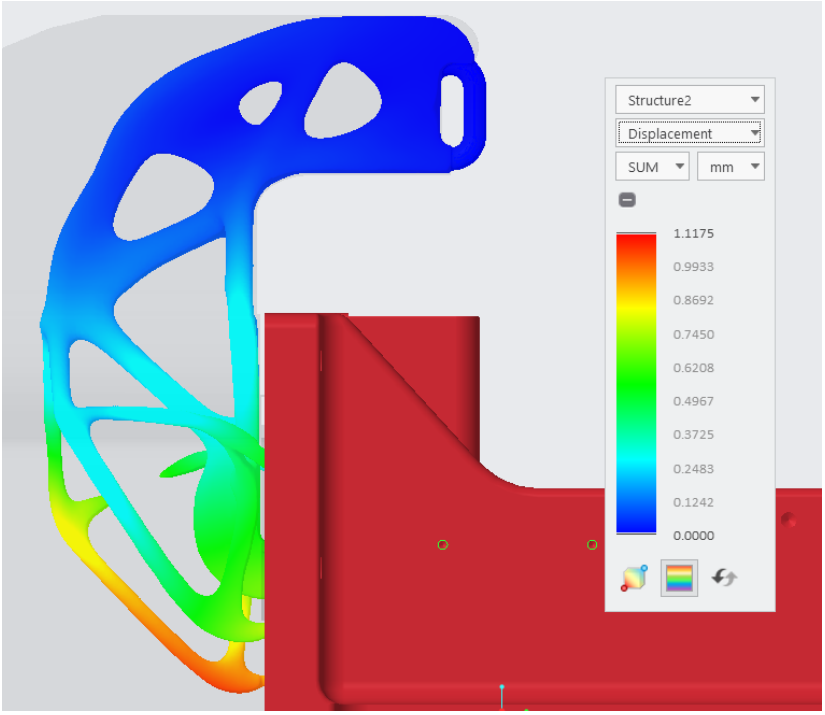

Figure 43 Lifting tool Design 1 TiAl4V maximum deformation

5.2 Case 2 Nozzle Holder Housing

5.2.1 Redesign

The nozzle holder housing is a challenging part, due to the many details both externally and internally. Topology optimization was not well suited for this, because the preserved bodies needed would be very complex. This is the reason optimization with lattices was chosen. The advantage of lattices is that all solid geometry can be replaced with a lightweight lattice structure, while preserving important features by replacing them with a shell. The material choice for the new part is 17-4PH du to its high yield strength at 1087 MPa.

The Nozzle holder housing was redesigned with a solid shell that preserved exterior and interior walls. The rest of the part was filled in with lattices. It was first attempted to create the shell and lattice within the lattice tool in Creo. However, this did not work, likely due to the geometry of the lattice structure being too complex. Instead, the shell was created manually by copying the existing geometry, similar to how preserved bodies are made for topology optimization. The original part was then replaced with beam lattices and merged with the shell. A section view of the nozzle holder housing with lattices is shown in Figure 44. The lattice is kept within a 2 mm thick shell that preserves all outer features. The part will be filled with powder when printed, therefore a small hole should be added to remove loose powder trapped inside. The infill in this part consists of star-shaped lattices and the beams have a diameter of 1,5 mm. The part in Figure 45 has lattices with uniform density. ANSYS did not seem to be able to handle the lattice structures, as they all disappeared when importing the part into ANSYS Mechanical. Fortunately Creo has a built-in simplified lattice function for simulation purposes that was used for the results of this case study.

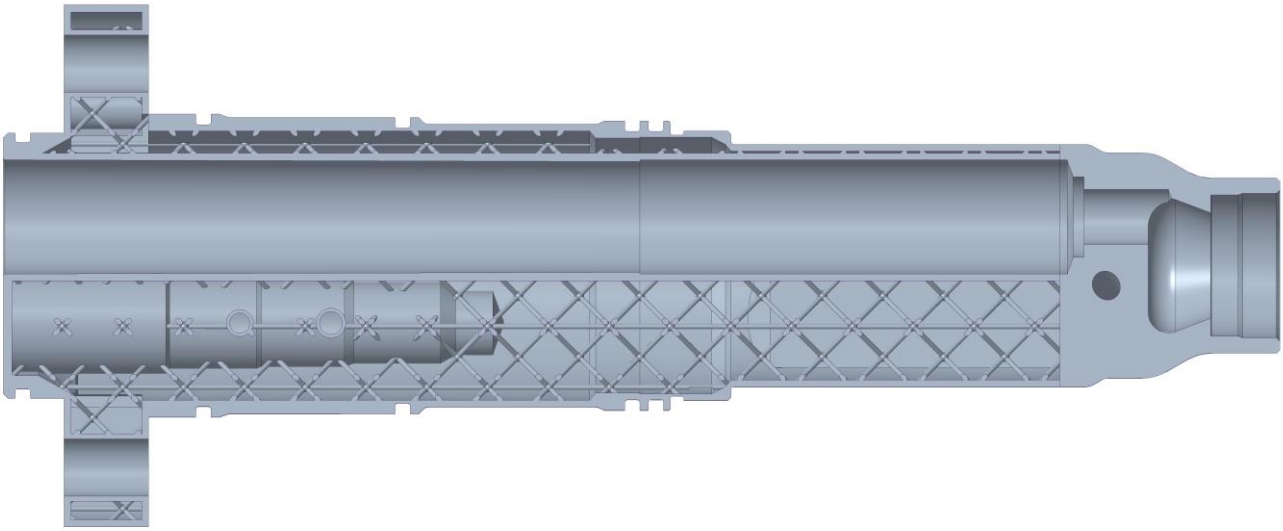

Figure 44 Nozzle holder housing Lattice view

A second version was created where the lattice density varies based on the simulation results of the original part. Areas with high stresses get more dense lattices, and low stress areas contain less dense lattices. Figure 45 shows the second version. This redesign is set to a maximum lattice density of 50% and quickly decreases down to only 2% density.

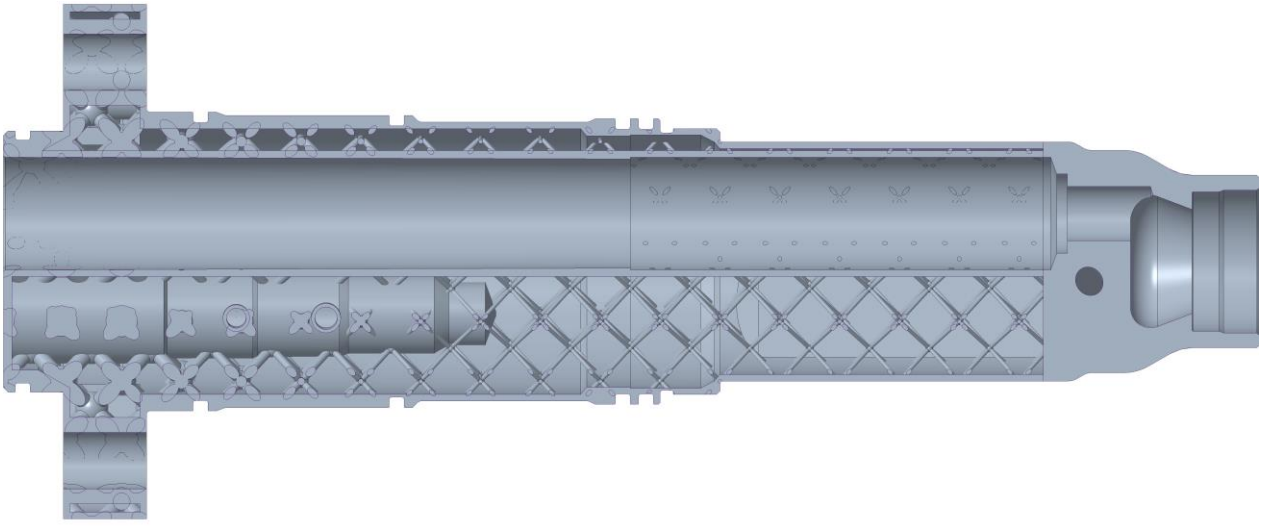

Figure 45 Nozzle holder housing Lattice with variable density

5.2.2 Results

Original nozzle holder housing GJS-500-7

The original nozzle holder housing weighs 9.82 kg. Simulation results from Creo show the maximum deformation is very small at 0.0155 mm and the maximum von mises stress is about 180 MPa, ignoring singularities. This is shown in Figure 46 andFigure 47.

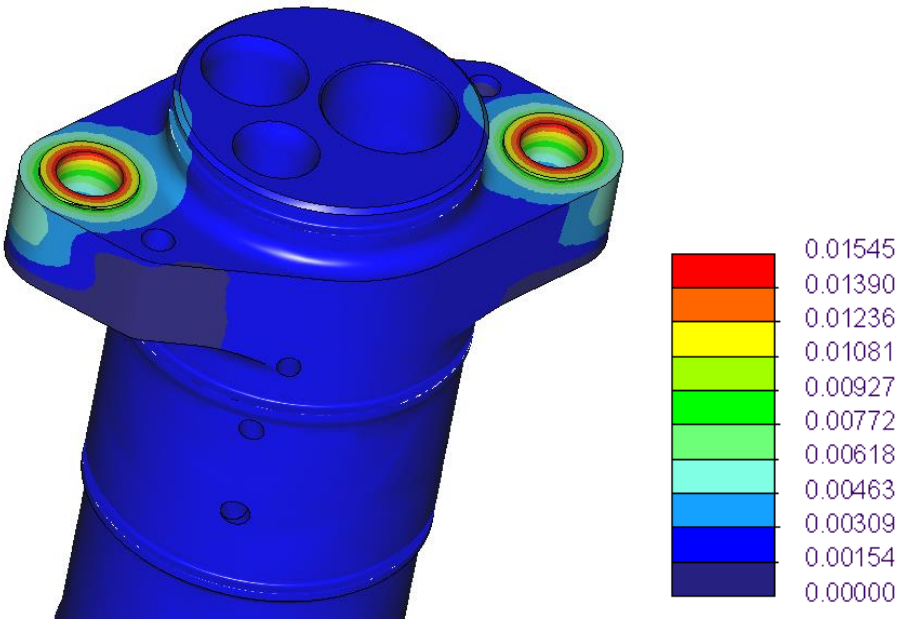

Figure 46 Nozzle holder housing Maximum deformation (mm)

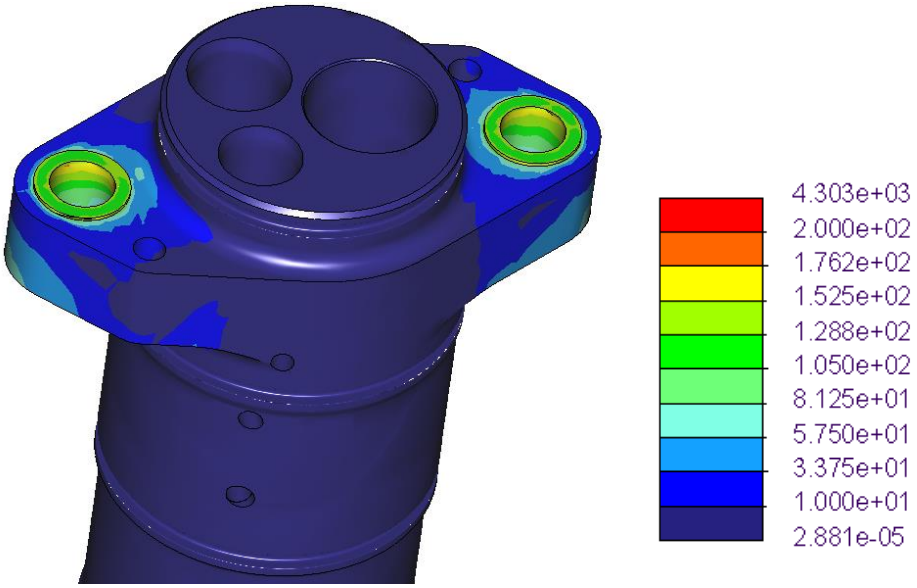

Figure 47 Nozzle holder housing von Mises stress (MPa)

Redesigned Nozzle holder housing 17-4PH

The first redesign with uniform lattice density has a weight of 4.4 kg. Figure 48 shows how the loads are distributed in the cylinder walls and lattices. The highest stresses are in the lattice beams where they connect with the shell or other beams, peaking at 375 MPa. Maximum deformation is 0.0186 mm from Figure 49, similar to the original part.

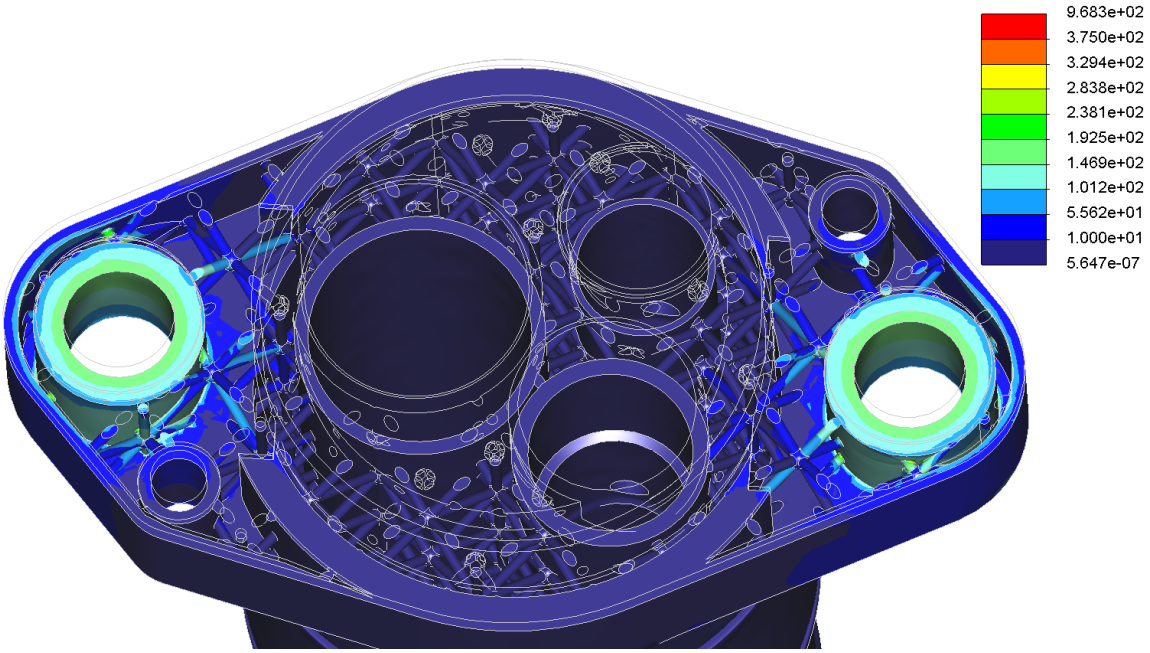

Figure 48 Nozzle holder housing von Mises stress (MPa), lattice view

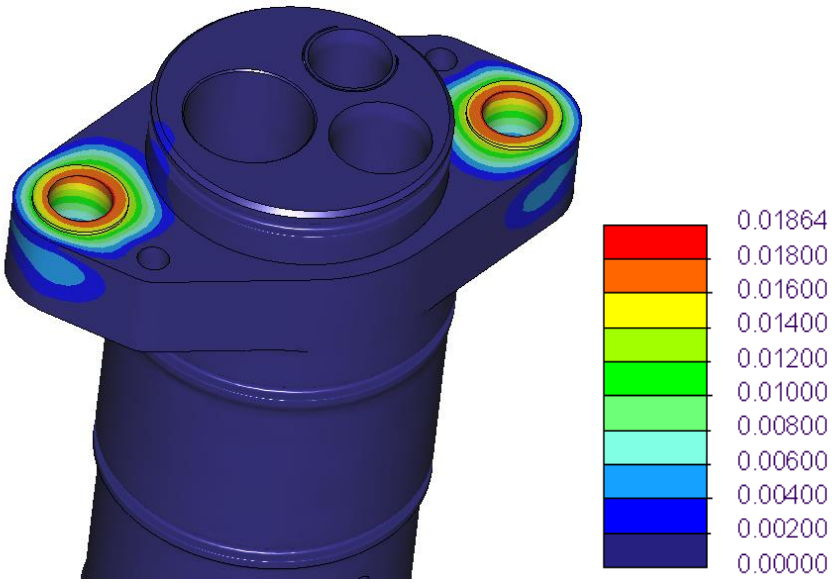

Figure 49 Nozzle holder housing Maximum deformation (mm)

The second redesign with variable density lattices weighs slightly more at 5.15 Kg. This is caused by the higher density and stronger lattices in the top part. The attempt to simulate the second version was unsuccessful. It can however be assumed that it is equally strong or stronger than the first version due to the high-density lattices. The cost of production is evaluated at 3112€.

5.3 Case 3 Injection cam follower redesign

5.3.1 Redesign

This part was challenging to optimize, as it had a lot of geometry that needed to be preserved, and therefore lower mass to include for optimization. A big challenge was to define the unnecessary volume. Enough mass had to be removed to replace it with steel without affecting the weight and functionality of the part. Three different redesigns have been created with various results.

5.3.2 Shell model

Because of its narrow and complicated geometry, using generative design in Creo is a challenge. A significant amount needs to be preserved, machined features, oil and lubrication channels, making optimization more difficult. Creating a hollowed-out model would seem to be a more effective option. In Ansys, both SpaceClaim and Discovery have a shell tool with the possibility of adding infill as well, making the part ready for general 3d-printing. On the first try, the new geometry created ended up with low-quality slicing, likely causing errors when trying to generate the mesh. As more trials and errors went on, it was discovered that this tool caused a horrible facet model of poor quality that Ansys did not approve of seen in Figure 50, leading to this approach being scrapped.

The first version was attempted using the lattice function in SpaceClaim. As mentioned earlier, this could have been a useful solution had it not been certain issues when generating the model. Spaceclaim's generation of hollowed out parts caused issues in Mechanical, getting errors saying the mesh generation did not complete due to poor quality elements. There were many attempts to change that and improve the elements without any success, and the same errors appeared.

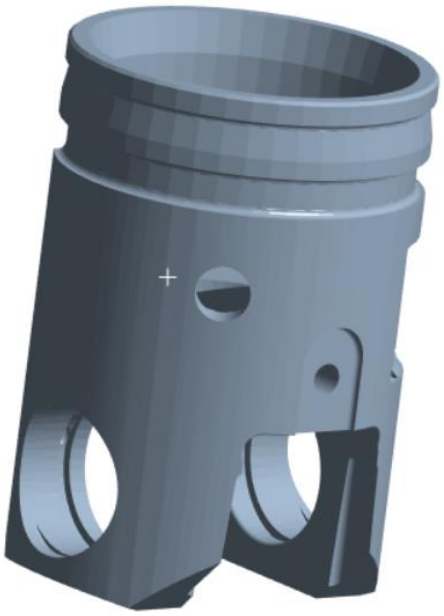

Figure 50 Injection cam follower Hollowed facet model

5.3.3 Topology optimization

A different and more promising approach was to return to Creo's generative design and keep the original at first, then assign the preserved geometry only to the bodies directly affected by the forces. Everything else left of the volume of the cylinder is left to the computer to decide what to make of and exclude. The thought was to later add a shell and rebuild what is necessary around the resulting optimized geometry.

However, it turned out it was much simpler to add all preserved bodies first, letting Creo integrate the new geometry into them. Before generating, the part needed to be rebuilt manually by copying the original part. The reason for this was when trying to optimize the original geometry, it ended up all clunky and with too high stress. Therefore, more human design interaction is still just as important as before, even though one is letting the computer do most of the work.

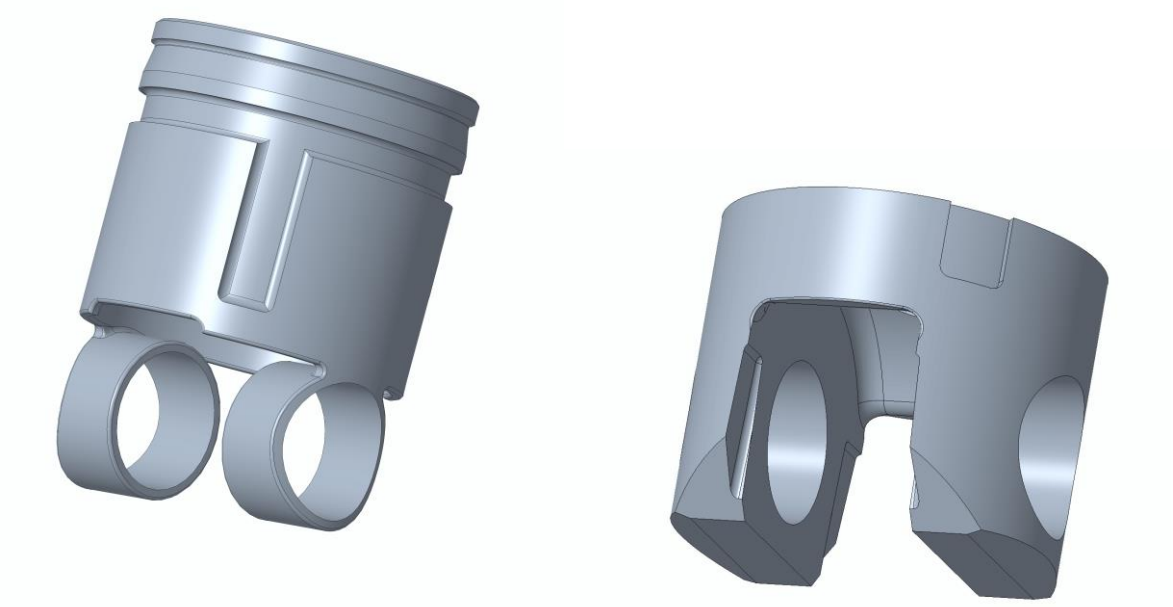

Figure 51 Injection cam follower Preserved and starting geometry

The geometry was split into parts; the top cylinder wall structure which would serve as preserved geometry, the internal platform where the fixed support is applied will also be part of the preserved geometry, and the lower body as starting geometry. Circular preserved bodies were also added to where the forces are applied to. The preserved body is shown in Figure 51. As mentioned earlier, choosing the build direction can be critical to avoid unnecessary support structures leading to rough surfaces. This geometry's build direction was set to top down since one would then avoid the overhanging structures more than 45 degrees of the lower part of the piston. Symmetry was applied to the vertical midplane after observing rods and material generation differences on each side which fixed the issue.

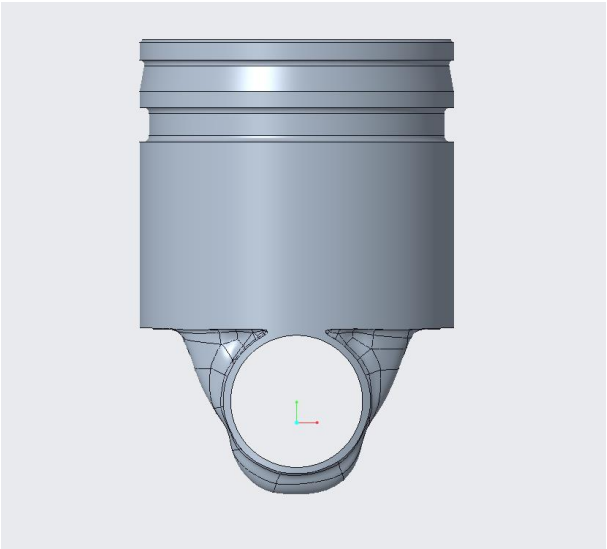

Figure 52 An experimental generated version

Several versions were generated after finding a lack of different adjustments or sorting out issues with generation, such as the one in
Figure 52. A problem that seemed to repeat was Creo freezing the optimization process when setting the fidelity over 2 with one of the computers used. This only seemed to be the case with this part. Eventually, the correct settings that provided the best results were found. The result was then generated as a new model with the highest quality of reconstruction. New issues arose after importing it into Ansys when generating the mesh, as Ansys refused to mesh any generated version of this part.

Figure 53 shows the final redesign for the topology optimization. The part was optimized for 316L steel, however this resulted in too much weight. The solution was to create a multimaterial part consisting of both aluminum alloy and steel.

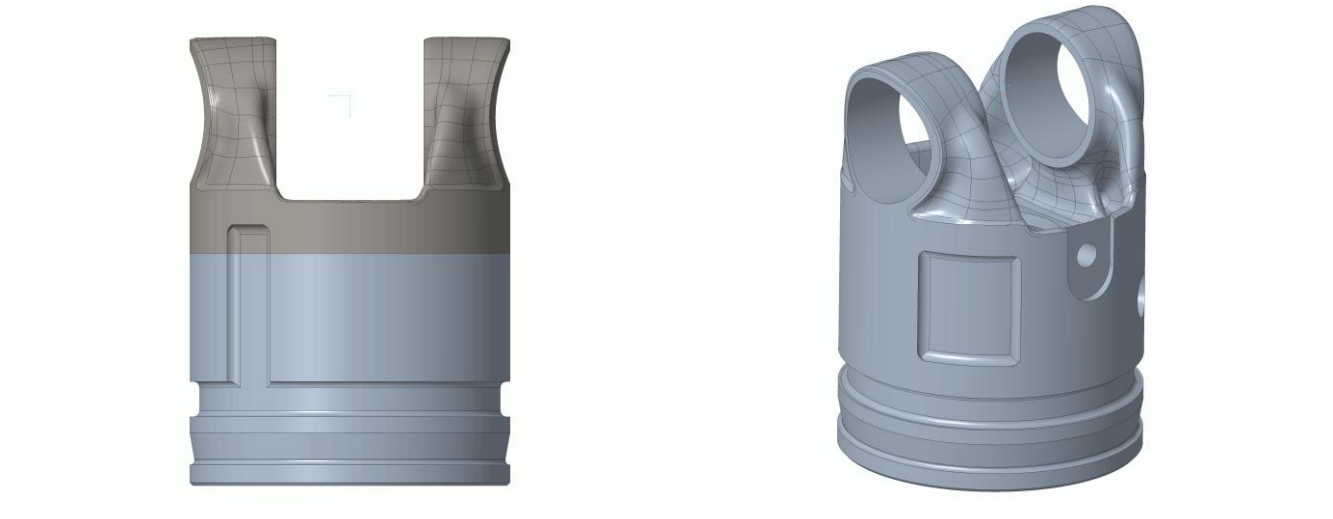

Figure 53 Top in 316L steel and bottom in AlSi10Mg

5.3.4 Modification of original geometry

The purpose of this redesign was to move and reorganize material in the areas where the cracks form, optimizing for aluminum to avoid increasing the weight. For the preparation of the geometry, extra material was added in said areas, and a recreation of the original was made with extra materials for Creo to use for its optimization process. This new approach attempted to make the program move around the material in the most optimal way, contrary to before where the purpose was to remove material for optimization.

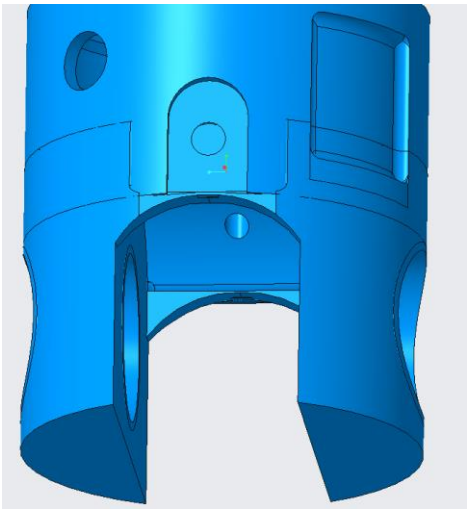

Figure 54 Injection cam follower Added geometry for TO

Figure 54 show the first attempt at modifying the geometry, but Creo was struggling to keep all the extrudes and bodies together as a part and every little tweak that was done brought errors to other extrudes or bodies. The rounding on the inside would not work, and the generated geometry did not fuse well together with the preserved and added geometry. Again, the geometry would not cooperate in Ansys with similar problems as mentioned before.

A new attempt was made, this time without the previous problems. The geometry was extended as much as possible and setup for mass optimization. The mass optimization did unfortunately not produce any meaningful improvements, results shown in Figure 55.

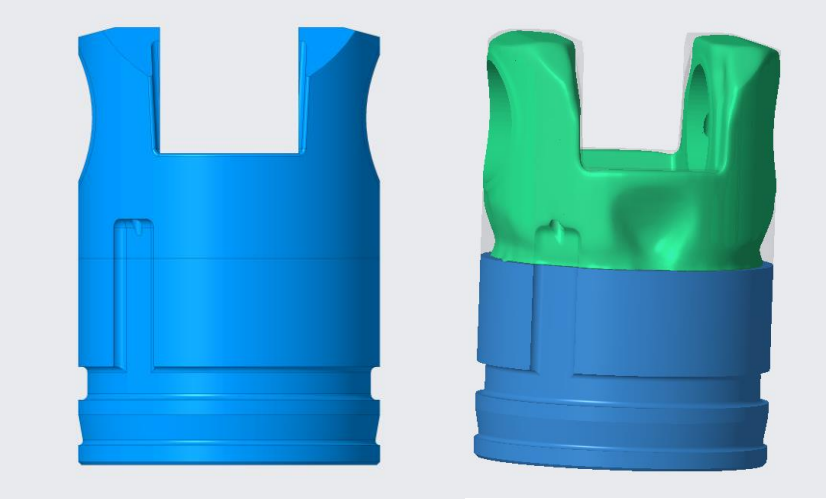

Figure 55 Injection cam follower Mass optimization

Another variant of this method was later found to manually modify the geometry to make it work better for the optimization process. By taking the original geometry and extending the cam roller cut-out, then optimizing with 99% mass to check stresses. After observing the location of the main stresses, curved extrusions were made to lower stress in the corners. This process was then repeated several times, until the geometry was rounded and modified enough to produce an acceptable result, shown in Figure 56.

Figure 56 Injection cam follower, new variant of modified geometry

5.3.5 Results

Original injection cam follower 6061 T6 force at 40 degrees

The result from the original part shows very high stresses compared to the fatigue limit of 90 MPa for the material 6061 T6. The highest principal stress of 176 MPa and 170 MPa can be found at the locations shown in Figure 57. High stresses were expected here as there is an issue with cracks forming in this area. Von mises stresses are generally high in all four corners seen in Figure 58, this is not as important for fatigue. The maximum deformation shown in Figure 59 is 0,223 mm.

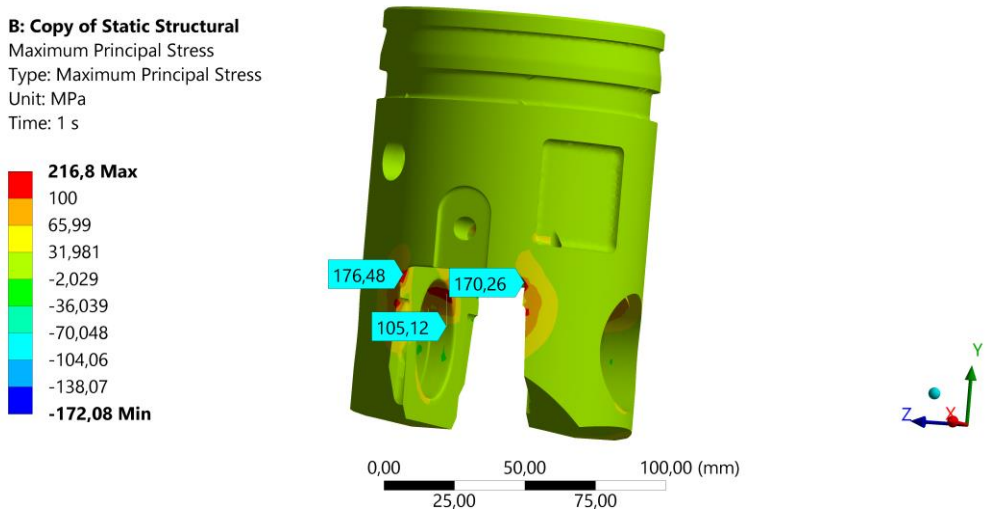

Figure 57 Injection cam follower Maximum principal stress

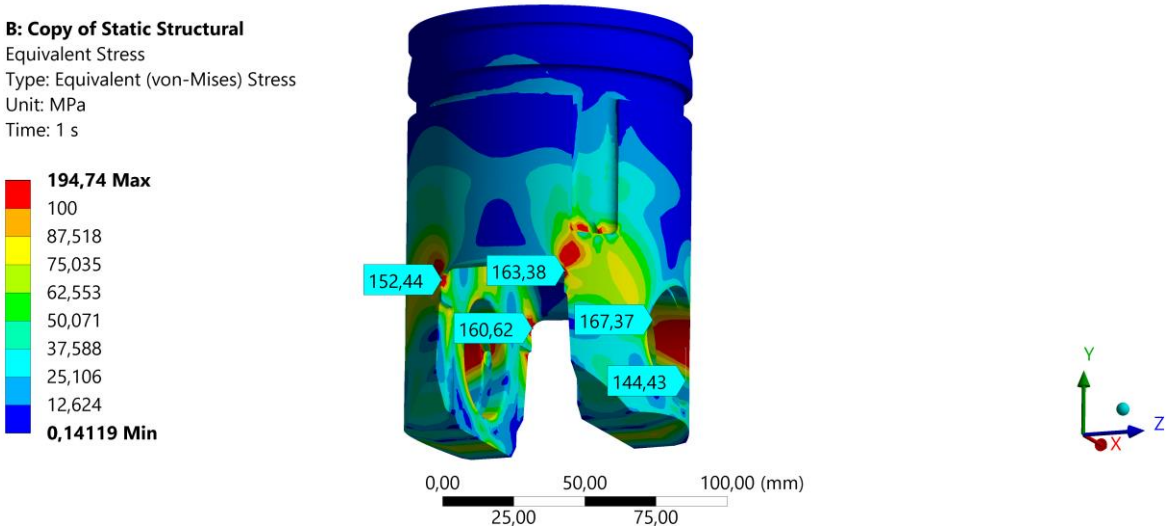

Figure 58 Injection cam follower von Mises stress

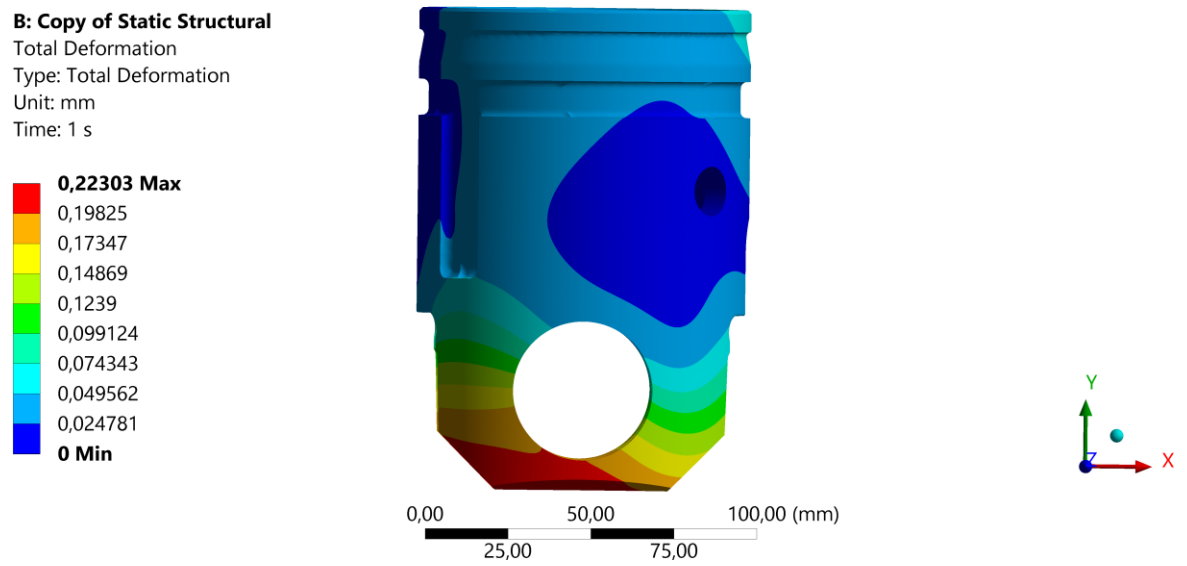

Figure 59 Injection cam follower Max deformation

Redesigned multimaterial version 316L and AlSi10Mg

One of the final versions ended up being a multi-material part with the top part being AlSi10Mg and the bottom optimized part being 316L. This was a result of seeing that a pure steel part resulted being significantly heavier despite the optimized design. Of the volume available for removing the mass, there simply were not enough volume to remove without negatively impacting the rest of the part in the design in terms of functionality. With a combination of AlSi10Mg as the top part and 316L as the bottom part which has a much higher fatigue limit at 340 MPa, one reduces the fatigue wear with a weight difference of only 10,17% more than the original. Deformation is shown below in Figure 60, and maximum principal and equivalent stress are shown in Figure 61 andFigure 62 respectively. The production cost of this part was estimated to be 1203€.

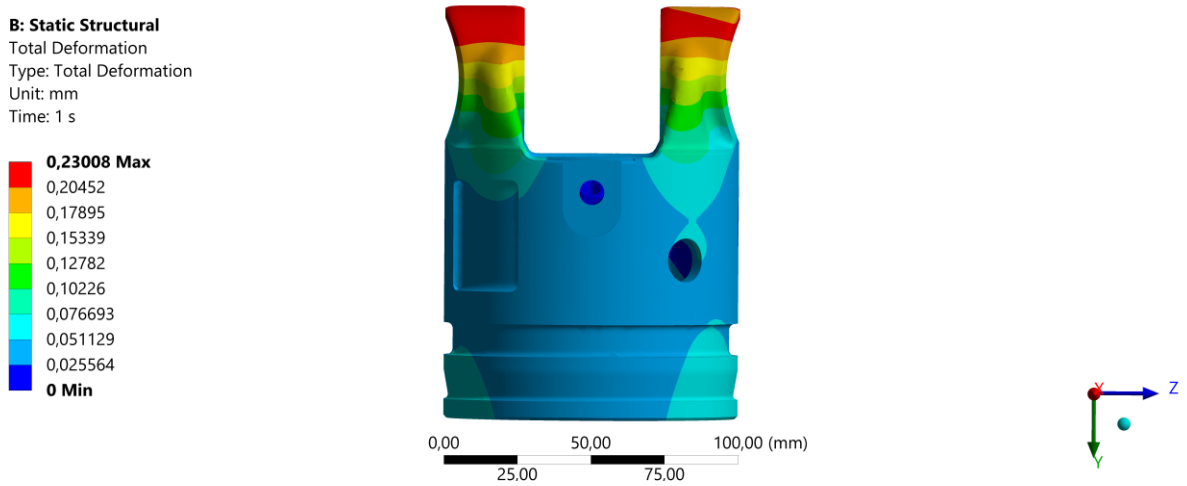

Figure 60 Injection cam follower Max deformation

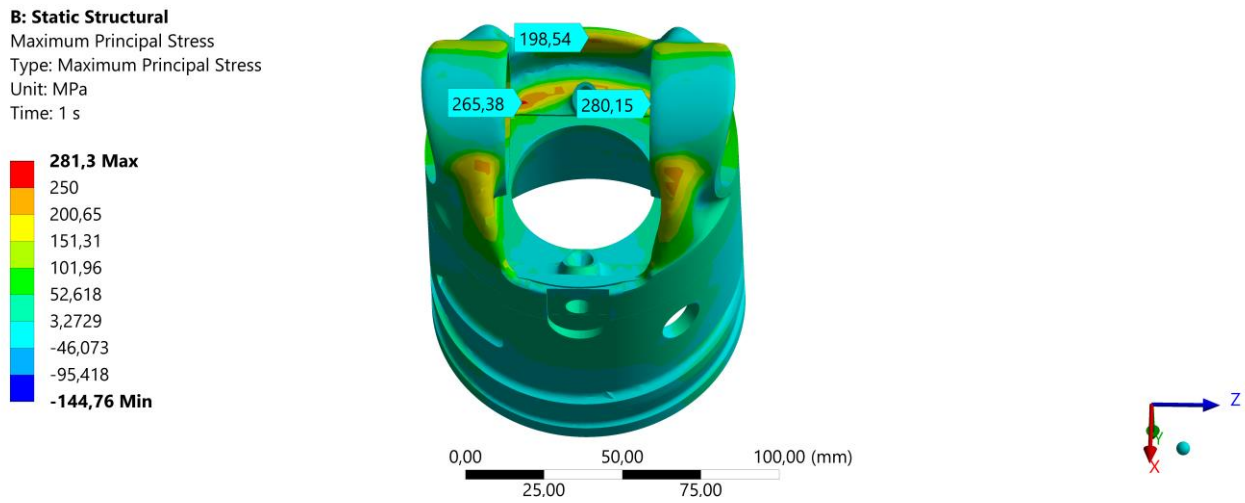

Figure 61 Injection cam follower Maximum principal stress

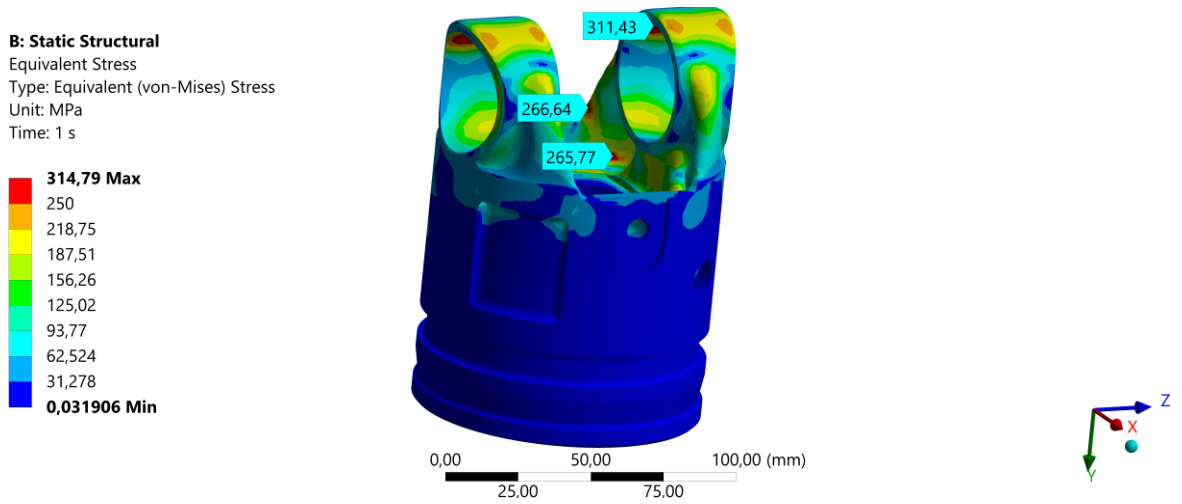

Figure 62 Injection cam follower von Mises stress

Modified geometry version AlSi10Mg

The last version that was made, was a manually modified version of the original. Both principal stresses and equivalent stresses were under 117 MPa shown in Figure 63 andFigure 64, much closer to the fatigue limit of 100 MPa than the original. The high stress concentrations in red are singularities appearing on the inside of the circular platform. The production cost of this version is estimated to be 1635€.

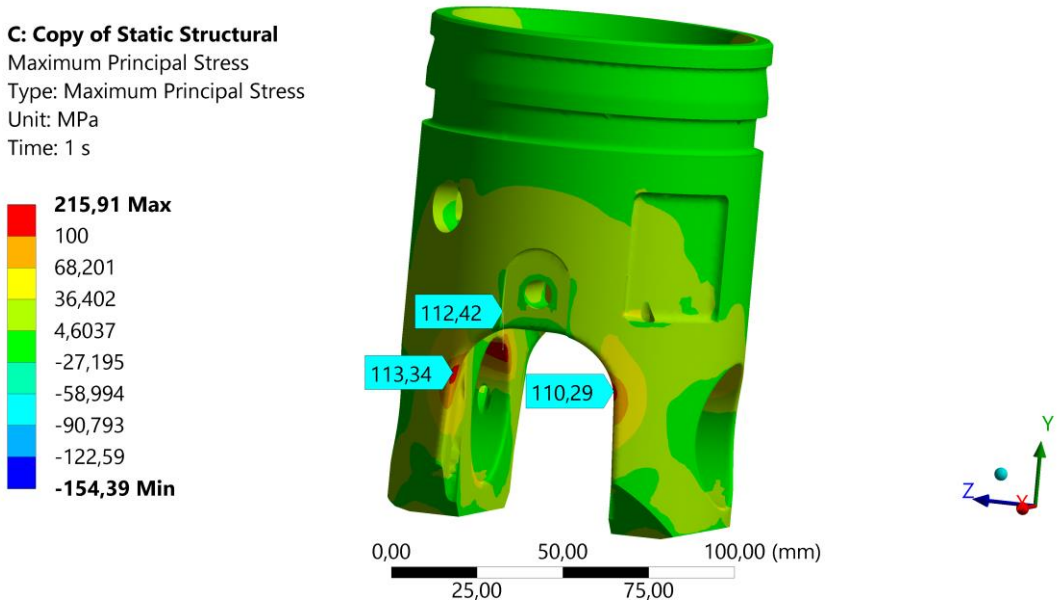

Figure 63 Injection cam follower Max principal stress

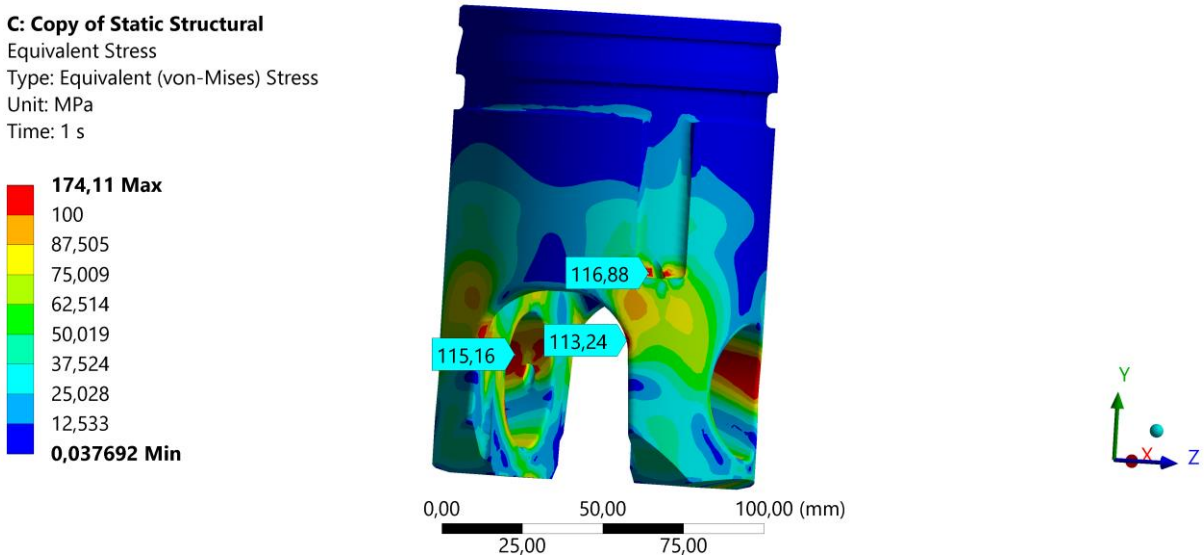

Figure 64 Injection cam follower von Mises stress

The deformation seen below in Figure 65 remained about the same as the original.

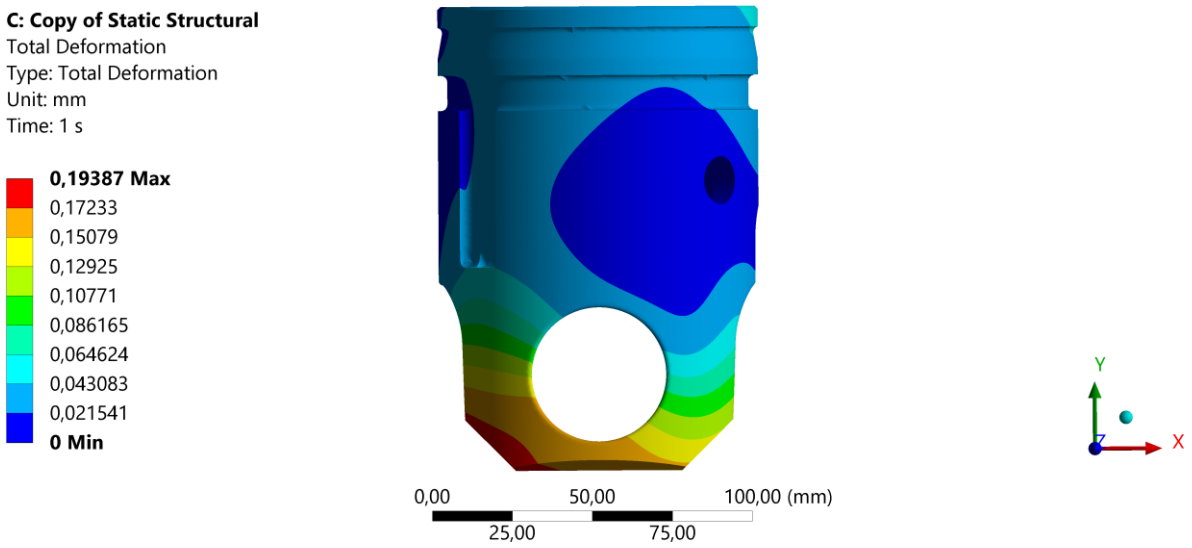

Figure 65 Injection cam follower Max deformation

5.4 Case 4 Valve Bridge

5.4.1 Redesign

To redesign the valve bridge with less weight and assemblies, topology optimization is used. The simple geometry and a large amount of available design space around the part makes it well suited for this type of optimization. The first step is to define the preserved bodies. This requires some manual modification of the geometry. The bolt and its cylinder are preserved in their original form, but the other bodies are modified with simpler and lighter parts, shown in Figure 66. The part is redesigned with 17-4PH, it has good mechanical properties and enables the middle head to be hardened. A version in titanium alloy is also created.

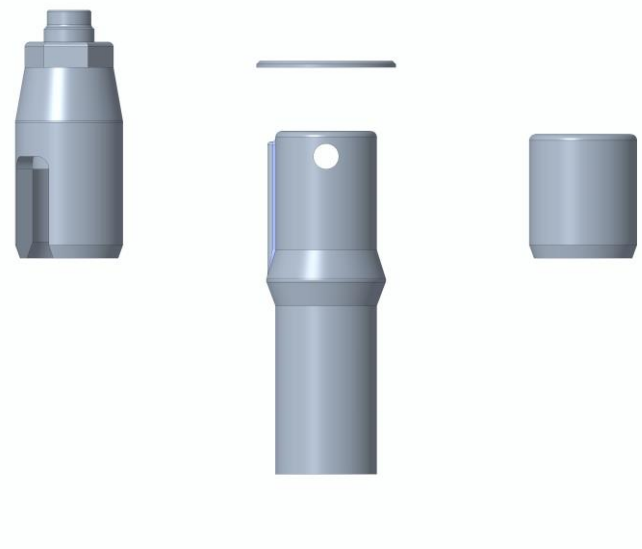

Figure 66 Valve bridge preserved bodies

Defining starting geometry was the next step. A large rectangular shape was created to fill the space surrounding the starting geometry, shown in Figure 67. Providing a big boundary that didn't restrict

where the material could be generated. The inside of the cylinders remained empty as no material should be generated there. Some chamfers and rounds were added to ensure a smooth transition between preserved body and the generated material.

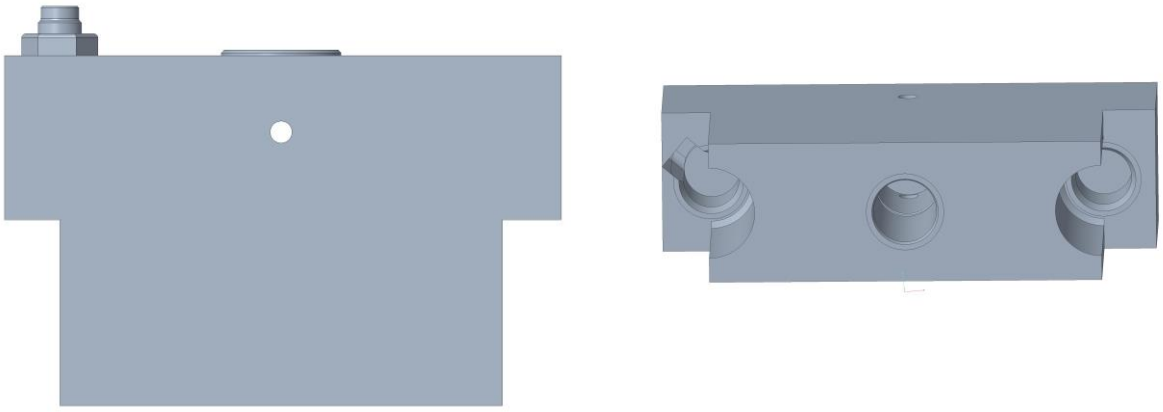

Figure 67 Valve bridge Starting geometry front and bottom view

The next step was to apply boundary conditions and settings for the topology optimization. Force and constraints remained the same as for the original part. The settings affected parameters such as weight, optimization quality and build direction. After optimization, the internal oil channel was added.

It was not a straightforward process from start to finish. It took several redesigns of starting and preserved geometry to get satisfying results. The figures below show some of the changes that were made during the optimization process.

The first version that was generated is shown in Figure 68. It was discovered that the red excluded geometry should be avoided as it did not get included in the simulation results. The preserved bodies could also be improved as they had a lot of unnecessary material.

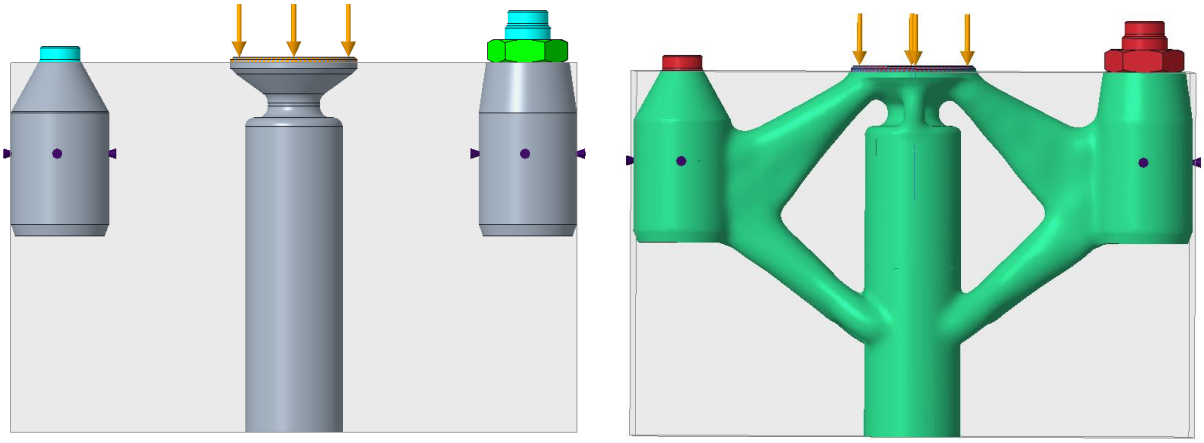

Figure 68 Valve bridge design attempt

For the second version, the preserved bodies have been reduced, allowing for better optimization. The boundary conditions changed slightly, however this resulted in an unsymmetric design, which was undesirable shown in Figure 70. Some generation issues also occurred, but this was fixed by modifying starting geometry and adding some chamfers and rounds to sharp edges.

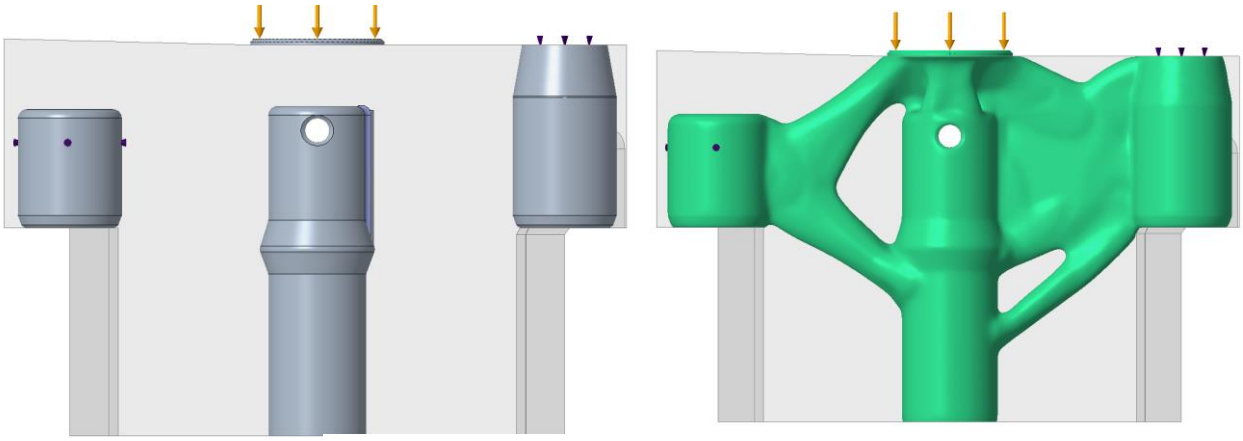

Figure 70 Valve bridge symmetry failure

Figure 71 shows the final valve bridge redesign.

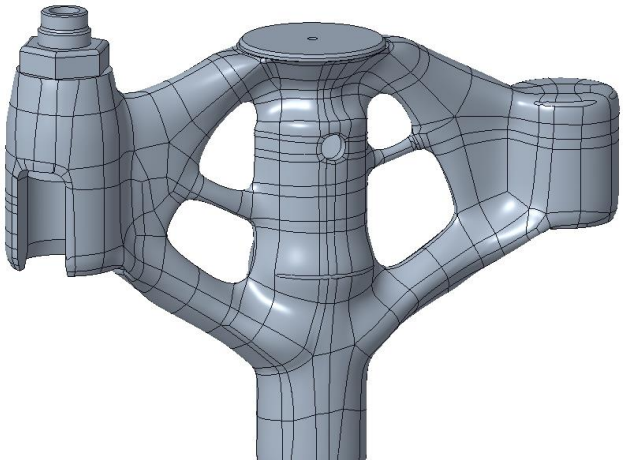

Figure 69 Valve bridge 17-4PH

5.4.2 Results

Original Valve Bridge GJS-500-7

The weight of the original part is 2,05 kg. Ignoring singularities, the highest equivalent stress is 156 MPa located inside the middle cylinder, shown in Figure 71. Figure 72 show similar principal stresses. The maximum deformation is 0,119 mm, seen in Figure 73.

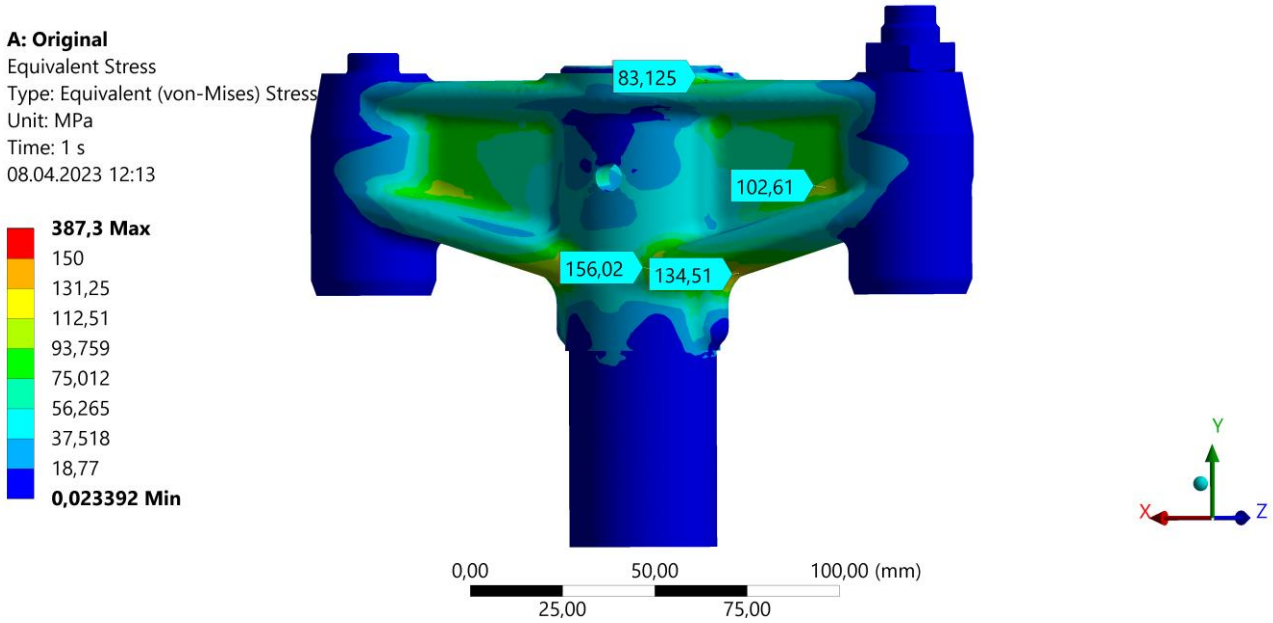

Figure 71 Original Valve bridge von Mises stress

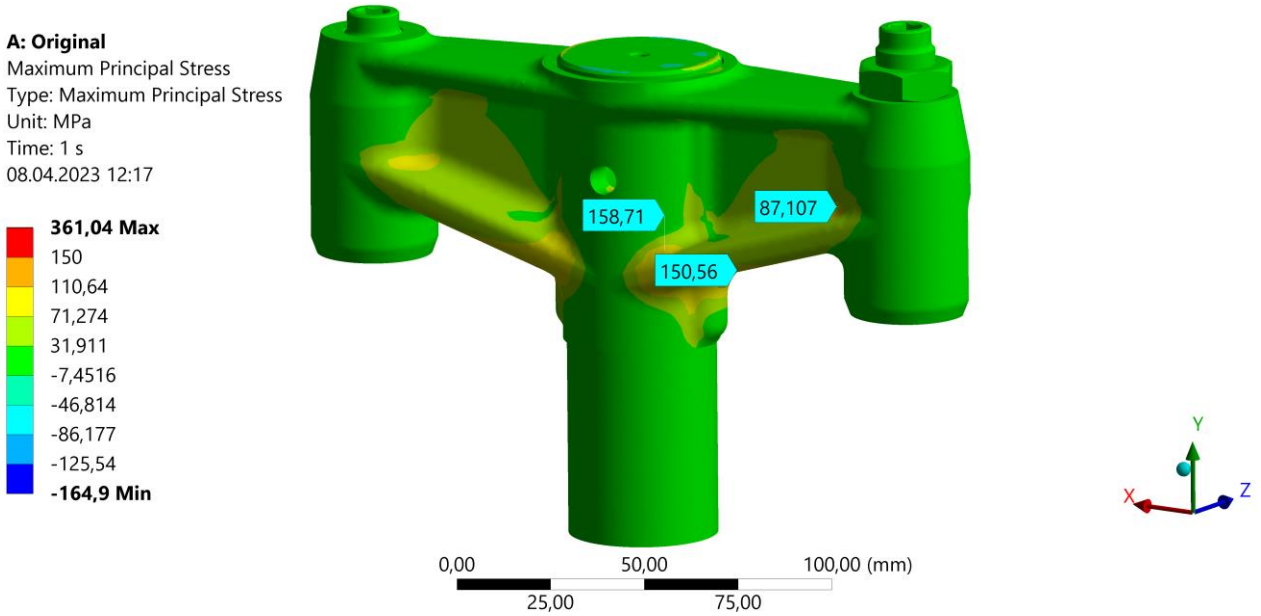

Figure 72 Valve bridge Principal stress

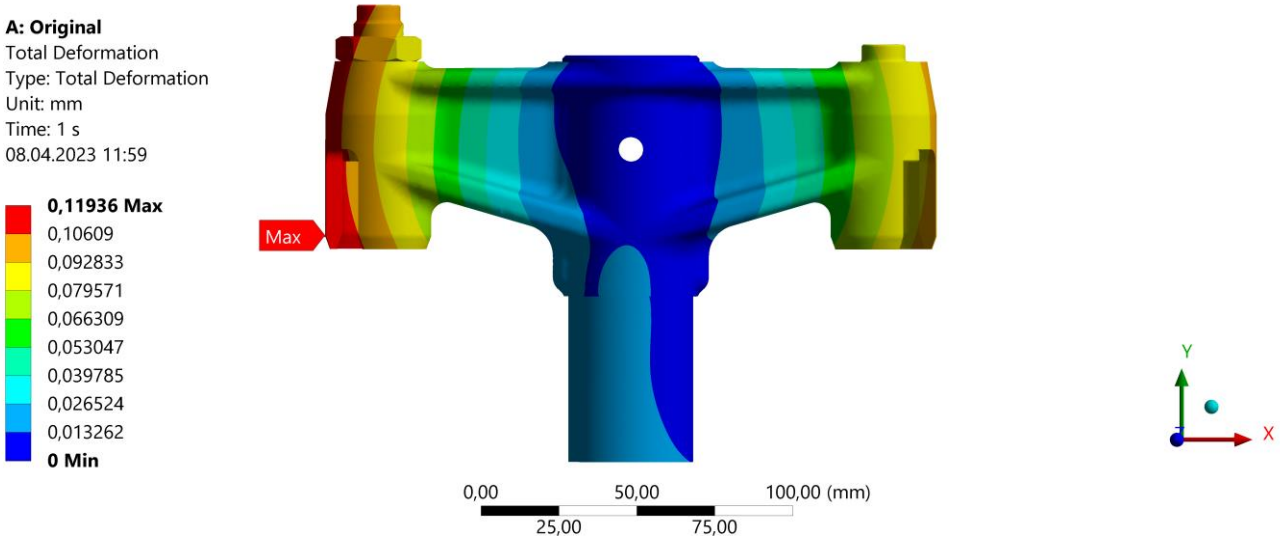

Figure 73 Original Valve bridge Max deformation

Redesigned Valve Bridge 17-4PH

The part with 17-4PH stainless steel weighs 1,43 kg, meaning 0,6 kg less than the original part. The assemblies have also been reduced, preserving only the adjustable bolt. Figure 75 shows the maximum principal stress of 219 MPa, located inside the cylinder similar to the original part. The von Mises stresses in Figure 74 are generally equal to the principal stresses, however the maximum von Mises stress of 226 MPa is located at the top. The deformation shown in Figure 76 is 0,107 mm. This was the limiting factor, as removing more material would increase the deformation above the 10 % limit. It would cost about 1156€ to produce.

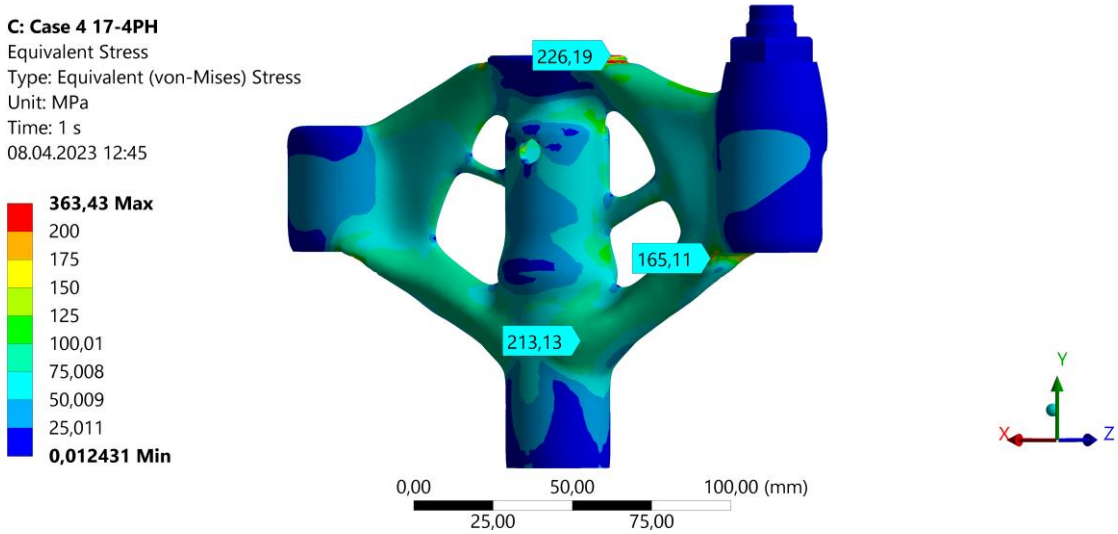

Figure 74 Optimized Valve bridge von Mises stress

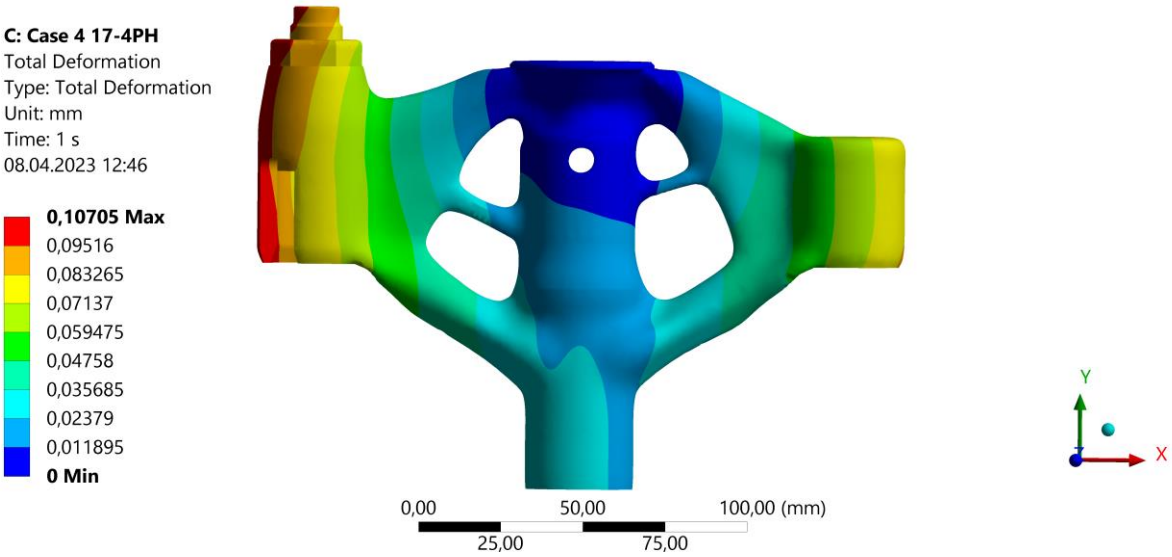

Figure 76 Optimized Valve bridge Max deformation

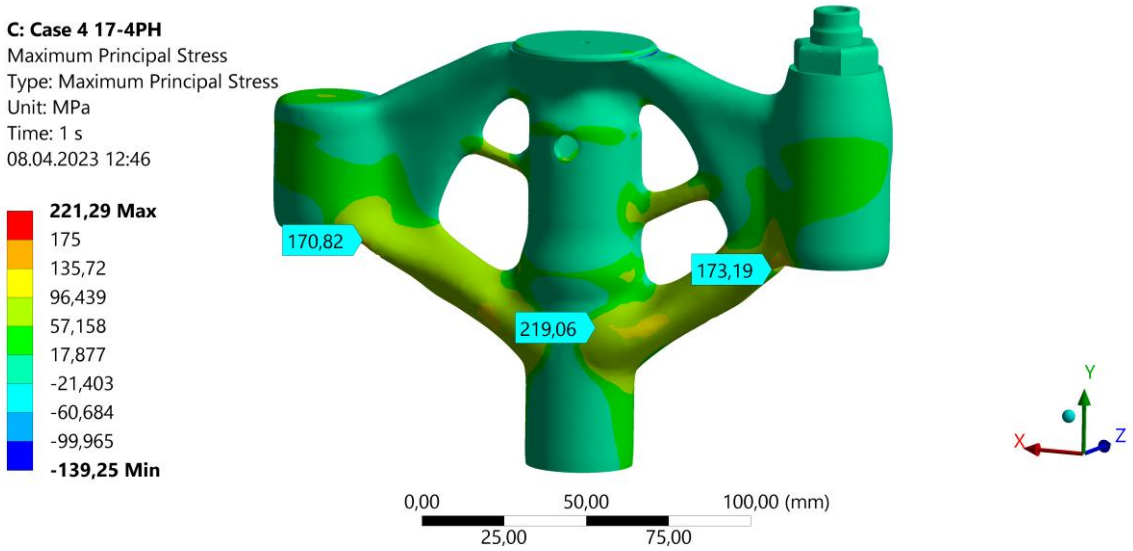

Figure 75 Optimized Valve bridge Principal stress

Redesigned valve bridge Ti-6Al-4V

In the more version with titanium alloy, the weight was only 0,974 kg. The low Young's modulus of Ti-6Al-4V compared to steel had a big impact on the results, the part reached the deformation limit well before the full strength of the material was utilized. Deformation was slightly higher than the original part shown in Figure 79 at 0,125 mm. Figure 77 and Figure 78 show the maximum stresses of 222 MPa principal stress and 302 MPa von Mises stress. These values are within the fatigue limit of 500 MPa. This version in titanium is estimated to cost 2156€.

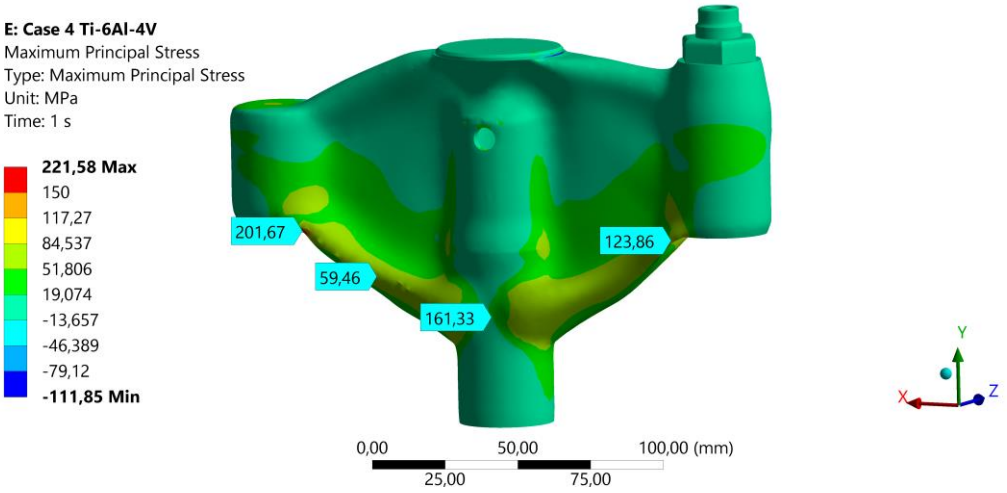

Figure 77 Optimized Valve bridge Ti-6Al-4V Principal stress

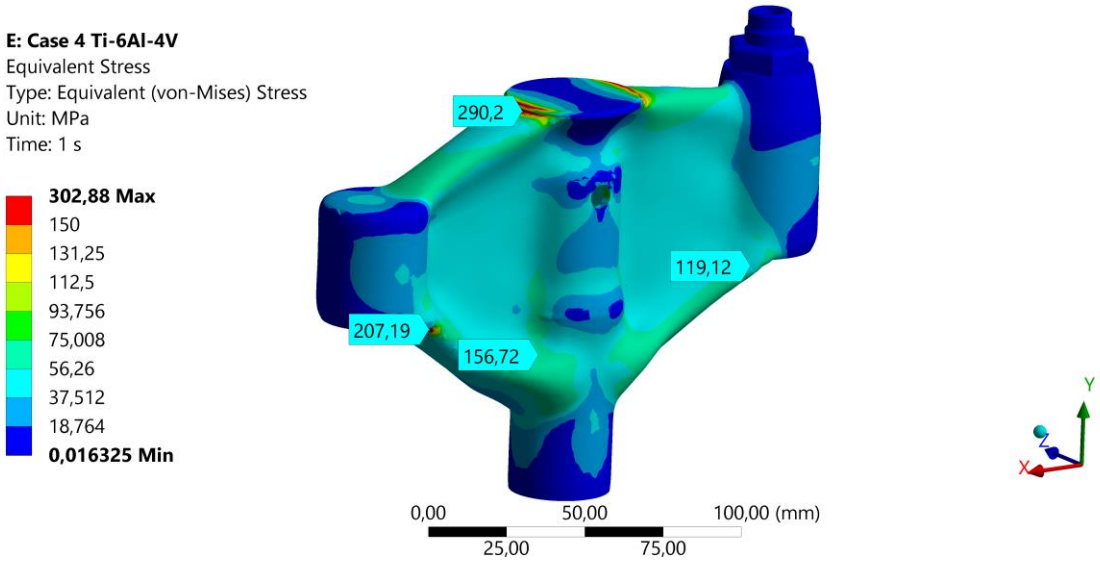

Figure 78 Optimized Valve bridge Ti-6Al-4V von Mises stress

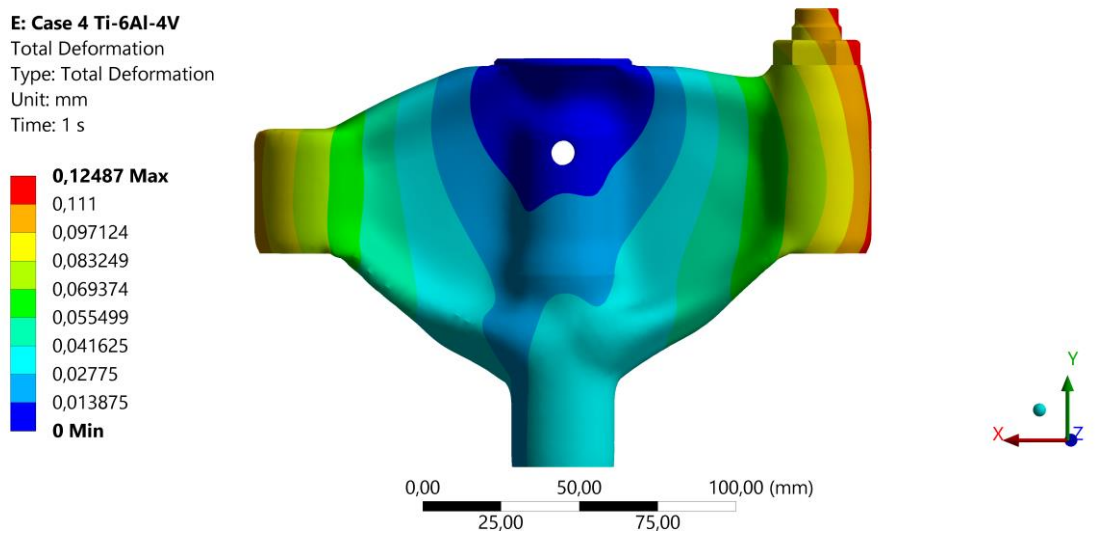

Figure 79 Optimized Valve bridge Ti-6Al-4V Max deformation

6. Discussion

6.1 Case 1, Lifting tool

As the purpose of this case was to produce something new with an AM mindset, there was no original part to start with or to compare. Topology optimization was the main design tool, making it possible to combine a simple, useful, and lightweight lifting tool without any need for assembly. After hooking the turbo foot up and the lifting procedure starts, the gravity force alone ensures it stays stable without creating any significant moment. Finding the center of gravity was crucial to design the supports and hooks for it to stay put with close to no pitch and roll motion.

The final design of this tool would be the last version, the hybrid between lifting tool versions 1 and 2. It has the lowest maximum stress and deformation and despite being slightly heavier than the one-support version 1, it offers much better stability and reliability when operating it, increasing its user friendliness. The final design will be the version made in aluminum, as it provides the highest strength to weight ratio. It has very low stresses, and a safety factor of 4,7 shown in Table 2.

Table 2: Comparing the lifting tool design 2 properties

Design 2 (one hooked)	**316L**	**Ti-Al-4V**	**AlSi10Mg**
Max von Mises stress (MPa)	78,3	54,4	60,4
Max deformation (mm)	0,3	0,39	0,7
Weight (kg)	3	1,9	1,1
Safety factor	6,2	18,2	10,6
Estimated price (€)	2149	3346	1846

The part in steel did not generate any successful results, and the titanium connected just barely all the points of stress, and one had to increase the weight to make Creo generate a somewhat reasonable result, leaving a part heavier than the aluminum. An alternative option is the version 1 in aluminum but with extra support extruded below to contribute to the lack of extra support version 1 have compared to version 2. The biggest advantage of the first version, is the much lower weight as shown in Table 3 where the aluminum is superior in nearly every aspect compared to steel and titanium.

Table 3: Comparing the lifting tool design 1 properties

Design 1 (three hooked)	**316L**	**Ti-Al-4V**	**AlSi10Mg**
Max von Mises stress (MPa)	N/A	96,8	74,5
Max deformation (mm)	N/A	1,1	1,01
Weight (kg)	N/A	2,46	2,5
Safety factor	N/A	10,2	
Estimated price (€)	N/A	6303	3237

As the first version with added support was printed, it was found that it did in fact increase stability drastically. For less than half the weight of the second version of the lifting tool, one only need to sacrifice a little bit of lateral stability, depending on preferences.

6.2 Case 2, Nozzle holder housing

The big potential of lattices is shown in this case, where significant weight savings was achieved without affecting the functionality. The optimization process was very simple, considering the complexity of the part. The limitations of topology optimization were discovered in case 3, and after defining the case with various assumptions and the information available, TO was simply not a viable option. Considering this part is only being exposed to a static load, fatigue stress is not an issue. Properties of each version shown in Table 4.

Table 4: Comparing the nozzle holder housing properties

Case 2 Results	GJS 500-7	Version 1 17-4PH	Version 2 17-4PH
Max von Mises stress (MPa)	180	375	N/A
Max deformation (mm)	0,0155	0,0186	N/A
Weight (Kg)	9,82	4,40	5,15
Weight saving (%)	N/A	55,2	47,6
Safety factor	1.7	2.9	N/A
Estimated price (€)	N/A	3112	N/A

6.3 Case 3, Injection cam follower

Looking at the topology optimized version of the cam follower, a great compromise of materials, weight and the restrictions given in this case turned out to be a multi-material combination of AlSi10Mg and 316L. After several trials of generating, there simply was not enough removable mass available for a pure steel part to remain about the same weight. Because of this, a viable solution was having only the bottom optimized part in steel while the rest of the part remained in aluminum. This made it possible to accept the stresses on the steel part. As the original aluminum part consistently had stresses about 70 MPa more than its fatigue limit, replacing that area with steel made the part less prone to fatigue wear. While the total stresses are a lot higher than in the original, the fatigue limit of 316L are much higher as well, capable of experiencing these stresses without surpassing the fatigue limit with a 10% extra weight as a trade-off. Another trade-off might be the probability of extra internal stresses due to the difference of thermal expansion between the materials.

After producing a finished design of the modified geometry version, the simulation numbers showed even better results. As shown in Table 5, not only is it approximately the same weight as the original also made in aluminum, but it has the lowest von Mises and principal stresses of them all. It might still be a bit over AlSi10Mg's fatigue limit at 100 MPa but observing the real-life effects of the stresses in the original, the lifespan should increase significantly.

Table 5: Comparing the injection cam follower properties

Case 3 results	Original (Al 6061)	AlSi10Mg+316L	Modified (AlSi10Mg)
Max von Mises stress (MPa)	166,94	284,96	111
Max principal stress (MPa)	176,13	300,92	112
Max deformation (mm)	0,19	0,23	0,2
Weight (kg)	0,95	1,05	0,96
Safety factor	1.57	1.62	2.24
Estimated price (€)	N/A	1203	1635

6.4 Case 4, Valve bridge

The valve bridge was successfully optimized as considerable weight savings and reduced assemblies were achieved. Comparing the results for the 17-4PH and Ti-Al6-4V version from Table 6, 17-4PH seems to provide the best result. It is both cheaper and have a better safety factor. The biggest advantage of the titanium version is its ability to achieve higher weight savings. However, the deformation limit, restricts the full utilization of the titanium alloy's strength.

Table 6: Comparing the valve bridge properties

Case 4 Results	**Original part**	**17-4PH**	**Ti-Al6-4V**
Max von Mises stress (MPa)	152	223	290
Max principal stress (MPa)	154	151	202
Max deformation (mm)	0,109	0,107	0,125
Weight (kg)	2,05	1,43	0,974
Weight savings (%)	N/A	30,2	52,5
Safety factor	2,1	4,90	3,4
Estimated price (€)	N/A	1156	2156

7. Conclusion

In this thesis, the objective was to reduce weight, improve design features and reduce fatigue stress using an AM mindset to see what was possible to come up with without being restricted by the traditional manufacturing processes. The parts that were redesigned were a nozzle holder housing, injection cam follower and a valve bridge. The lifting tool was designed from the bottom without any reference design, as the goal was to see what design an AM mindset would produce. All information and models were provided by Bergen Engines.

Two of the parts were made significantly lighter and with safety factors well over their minimum criteria when designed in the optimized AM metal counterparts such as 17-4PH and AlSi10Mg. One part remained about the same weight with better fatigue resistance, and one was made simple and light enough for one person to operate with optimal stability. Errors and issues caused by Creo and ANSYS that resulted in limitations in the analysis and results were discussed, and alternative solutions were implemented.

The results from the case studies show that topology and lattice optimization can in many cases lead to significant weight savings and simplified designs. These designs are enabled by AM, this can however lead to challenges with high part costs.

For future projects, it would be interesting to compare other software optimization capabilities, such as topology and lattice optimization. Also, to find more effective methods for analyzing parts designed for AM.

8. References

[1] "About," *Bergen Engines*. https://www.bergenengines.com/about/ (accessed Mar. 28, 2023).

[2] I. Gibson, D. Rosen, B. Stucker, M. Khorasani, *Additive Manufacturing Technologies*. Springer Nature Switzerland AG, 2021. doi: 10.1007/978-3-030-56127-7.

[3] D. Herzog, V. Seyda, E. Wycisk, og C. Emmelmann, «Additive manufacturing of metals», *Acta Mater*, vol. 117, p. 371–392, sep. 2016, doi: 10.1016/j.actamat.2016.07.019.

[4] L. Carneiro, B. Jalalahmadi, A. Ashtekar, og Y. Jiang, «Cyclic deformation and fatigue behavior of additively manufactured 17–4 PH stainless steel», *Int. J. Fatigue*, vol. 123, p. 22–30, jun. 2019, doi: 10.1016/j.ijfatigue.2019.02.006.

[5] H. D. Nguyen *mfl.*, «A critical review on additive manufacturing of Ti-6Al-4V alloy: microstructure and mechanical properties», *J. Mater. Res. Technol.*, vol. 18, p. 4641–4661, may 2022, doi: 10.1016/j.jmrt.2022.04.055.

[6] "Steel vs Superalloys - Comparison - Pros and Cons," *Material Properties*, Jul. 31, 2020. https://material-properties.org/steel-vs-superalloys-comparison-pros-and-cons/ (accessed Mar. 28, 2023).

[7] R. Shrestha, J. Simsiriwong, og N. Shamsaei, «Fatigue behavior of additive manufactured 316L stainless steel parts: Effects of layer orientation and surface roughness», *Addit. Manuf.* ,vol. 28, p. 23–38, aug. 2019, doi: 10.1016/j.addma.2019.04.011.

[8] M. Mahmoudi, A. Elwany, A. Yadollahi, S. M. Thompson, L. Bian, and N. Shamsaei, "Mechanical properties and microstructural characterization of selective laser melted 17-4 PH stainless steel," *Rapid Prototyp. J.*, vol. 23, no. 2, pp. 280–294, Jan. 2017, doi: 10.1108/RPJ-12-2015-0192.

[9] "Spheroidal graphite iron." https://www.vonroll-casting.ch/en/spheroidal-graphite-iron.html (accessed Mar. 28, 2023).

[10] "ASM Material Data Sheet." https://asm.matweb.com/search/SpecificMaterial.asp?bassnum=ma6061t6 (accessed Mar. 28, 2023).

[11] A. Raja, S. R. Cheethirala, P. Gupta, N. J. Vasa, and R. Jayaganthan, "A review on the fatigue behaviour of AlSi10Mg alloy fabricated using laser powder bed fusion technique," *J. Mater. Res. Technol.*, vol. 17, pp. 1013–1029, Mar. 2022, doi: 10.1016/j.jmrt.2022.01.028.

[12] H. Hegab, N. Khanna, N. Monib, og A. Salem, «Design for sustainable additive manufacturing: A review», *Sustain. Mater. Technol.*, vol. 35, apr. 2023, doi: 10.1016/j.susmat.2023.e00576.

[13] O. Diegel, A. Nordin, and D. Motte, *A Practical Guide to Design for Additive Manufacturing*. Singapore doi: 10.1007/978-981-13-8281-9.

[14] M. J, “Topology optimization for 3D printing,” *3Dnatives*, Dec. 09, 2020. https://www.3dnatives.com/en/topology-optimisation140820184/ (accessed May 12, 2023).

[15] C. S. Andreasen, M. O. Elingaard, and N. Aage, “Level set topology and shape optimization by density methods using cut elements with length scale control,” *Struct. Multidiscip. Optim.*, vol. 62, no. 2, pp. 685–707, Aug. 2020, doi: 10.1007/s00158-020-02527-1.

[16] “Guide to lattice structures in additive manufacturing,” *nTop*. https://www.ntop.com/resources/blog/guide-to-lattice-structures-in-additive-manufacturing (accessed May 10, 2023).

[17] A. Nazir *mfl.*, «Multi-material additive manufacturing: A systematic review of design, properties, applications, challenges, and 3D printing of materials and cellular metamaterials», *Mater. Des.*, . 226, p. 111661, feb. 2023, doi: 10.1016/j.matdes.2023.111661.

[18] E. M. Sefene, Y. M. Hailu, and A. A. Tsegaw, “Metal hybrid additive manufacturing: state-of-the-art,” *Prog. Addit. Manuf.*, vol. 7, no. 4, pp. 737–749, Aug. 2022, doi: 10.1007/s40964-022-00262-1.

[19] “What is Ultrasonic Additive Manufacturing?” https://www.twi-global.com/technical-knowledge/faqs/what-is-ultrasonic-additive-manufacturing.aspx (accessed Apr. 30, 2023).

[20] "Fabrisonic". https://fabrisonic.com/ultrasonic-additive-manufacturing-overview/ (accessed Apr. 30, 2023).

[21] «Creo - Analysis software by PTC | DirectIndustry». https://www.directindustry.com/prod/ptc/product-14603-1761769.html (accessed May.19, 2023]

[22] «FEA Software Definition with Simulation Examples». https://www.comsol.com/multiphysics/fea-software (accessed May.19, 2023).

[23] “New Version of PTC’s Award-Winning CAD Platform Introduces a Renaissance in Design,” Mar. 19, 2019. https://www.businesswire.com/news/home/20190319005836/en/New-Version-of-PTC%E2%80%99s-Award-Winning-CAD-Platform-Introduces-a-Renaissance-in-Design (accessed May 19, 2023).

List of figures

Figure 1 Illustration of PBF process [2, p.126] 3
Figure 2 Four types of lattice structures [16] 7
Figure 3 Periodic machining operations [20] 9
Figure 4 Bonding a metal strip to the base plate with UAM [20] 9
Figure 5 Topology optimization process [21] 10
Figure 6 Flow chart of the optimization process 11
Figure 7 Example of a sliced part 12
Figure 8 Illustration of a FE analysis [22] 13
Figure 9 Example use of lattice in Creo [23] 13
Figure 10 Lifting procedure for turbocharger foot 14
Figure 11 Nozzle holder housing original part 15
Figure 12 Nozzle holder housing, load and constraint highlighted in green 15
Figure 13 Injection cam follower, Original part 16
Figure 14 The real-life model with the strained areas visible 16
Figure 15 Injection cam follower Applied force 17
Figure 16 Injection cam follower Fixed support placement 17
Figure 17 Original valve bridge 18
Figure 18 Valve bridge Fixed support 19
Figure 19 Valve bridge Load 19
Figure 20 Lifting tool, preserved bodies to the left, starting geometry to the right 20
Figure 21 Lifting tool, Preserved bodies to the left, starting geometry to the right 21
Figure 22 Lifting tool Hinge design 21
Figure 23 Lifting tool Design 2 316L 22
Figure 24 Lifting tool Design 2 316L von Mises stress 23
Figure 25 Lifting tool Design 2 316L Max deformation 23
Figure 26 Lifting tool Design 2 Ti-Al6-4V von Mises stress 24
Figure 27 Lifting tool Design 2 Ti-Al6-4V Max deformation 24

Figure 28 Lifting tool Design 2 AlSi10Mg von Mises stress 25
Figure 29 Lifting tool Design 2 AlSi10Mg Max deformation 25
Figure 30 Stability support added to Lifting tool design 2 AlSi10Mg 26
Figure 31 Lifting tool Design 1 AlSi10Mg 27
Figure 32 Lifting tool Design 1 AlSi10Mg von Mises stress 27
Figure 33 Lifting tool design 1 AlSi10Mg von Mises stress 28
Figure 34 Lifting tool Design 1 AlSi10Mg Maximum deformation 28
Figure 35 Initial hinge, Lifting tool design 1 29
Figure 36 Lifting tool Design 1 AlSi10Mg, improved version 29
Figure 37 Lifting tool Design 1 improved AlSi10Mg von Mises stress, load case 1 30
Figure 38 Lifting tool Design 1 improved AlSi10Mg Maximum deformation, load case 1 30
Figure 39 Lifting tool Design 1 AlSi10Mg improved von Mises stress, load case 2 31
Figure 40 Lifting tool Design 1 improved Maximum deformation, load case 2 31
Figure 41 Lifting tool Design 1 improved unsuccessful with 316L 32
Figure 42 Lifting tool Design 1 improved TiAl4V von Mises stress 32
Figure 43 Lifting tool Design 1 TiAl4V maximum deformation 33
Figure 44 Nozzle holder housing Lattice view 34
Figure 45 Nozzle holder housing Lattice with variable density 34
Figure 46 Nozzle holder housing Maximum deformation (mm) 35
Figure 47 Nozzle holder housing von Mises stress (MPa) 35
Figure 48 Nozzle holder housing von Mises stress (MPa), lattice view 36
Figure 49 Nozzle holder housing Maximum deformation (mm) 36
Figure 50 Injection cam follower Hollowed facet model 37
Figure 51 Injection cam follower Preserved and starting geometry 38
Figure 52 An experimental generated version 38
Figure 53 Top in 316L steel and bottom in AlSi10Mg 39
Figure 54 Injection cam follower Added geometry for TO 39
Figure 55 Injection cam follower Mass optimization 40

Figure 56 Injection cam follower, new variant of modified geometry 40
Figure 57 Injection cam follower Maximum principal stress 41
Figure 58 Injection cam follower von Mises stress 41
Figure 59 Injection cam follower Max deformation 42
Figure 60 Injection cam follower Max deformation 42
Figure 62 Injection cam follower Maximum principal stress 43
Figure 63 Injection cam follower von Mises stress 43
Figure 64 Injection cam follower Max principal stress 44
Figure 65 Injection cam follower von Mises stress 44
Figure 66 Injection cam follower Max deformation 45
Figure 67 Valve bridge preserved bodies 45
Figure 68 Valve bridge Starting geometry front and bottom view 46
Figure 69 Valve bridge design attempt 46
Figure 71 Valve bridge 17-4PH 47
Figure 70 Valve bridge symmetry failure 47
Figure 72 Original Valve bridge von Mises stress 48
Figure 73 Valve bridge Principal stress 48
Figure 74 Original Valve bridge Max deformation 49
Figure 75 Optimized Valve bridge von Mises stress 49
Figure 76 Optimized Valve bridge Principal stress 50
Figure 77 Optimized Valve bridge Max deformation 50
Figure 78 Optimized Valve bridge Ti-6Al-4V Principal stress 51
Figure 79 Optimized Valve bridge Ti-6Al-4V von Mises stress 51
Figure 80 Optimized Valve bridge Ti-6Al-4V Max deformation 51

List of tables

Table *1*: Material properties 5

Table 2: Comparing the lifting tool design 2 properties 52

Table 3: Comparing the lifting tool design 1 properties 52

Table 4: Comparing the nozzle holder housing properties 53

Table 5: Comparing the injection cam follower properties 53

Table 6: Comparing the valve bridge properties 54